GeoScienceWorld
Lithosphere
Volume 2023, Article ID lithosphere_2023_229, 22 pages
https://doi.org/10.2113/2023/lithosphere_2023_229

Lithosphere

Research Article

A Long-Lived Accretionary Process during the Amalgamation of the North China Craton: Insights from Neoarchean–Paleoproterozoic Polyphase Magmatism in the Lüliang Complex

Xinyuan Yu,[1] Jian Zhang,[1,2] Jin Liu,[3] Changqing Yin,[1] Ying Chen,[1] Minjie Guo,[1] Jiahui Qian,[1] Peng Gao,[1] and Changquan Cheng[1]

[1]*School of Earth Sciences and Engineering, Sun Yat-sen University, Guangzhou 510275, China*
[2]*Department of Earth Sciences, The University of Hong Kong, Pokfulam Road, Hong Kong SAR*
[3]*College of Earth Sciences, Jilin University, Changchun 130061, China*

Correspondence should be addressed to Jian Zhang; zhangjian@mail.sysu.edu.cn

Received 14 July 2023; Accepted 17 October 2023; Published 14 November 2023

Academic Editor: Songjian Ao

There has been a long debate regarding the timing of the final amalgamation of the North China Craton, which is considered to have occurred either during the Neoarchean or Paleoproterozoic era. One major point of contention is whether there existed a long-lived subduction lasting through the Neoarchean to Paleoproterozoic. The Lüliang Complex contains multiphases of magmatism and thus represents the most viable region to address this controversy. In this study, we carried geochronological and geochemical analysis on the representative granitoids. Secondary ion mass spectrometry U–Pb dating revealed four distinct granitoid groups emplaced at 2531 ± 4, 2189–2173, 2027 ± 25, and 1852 ± 41 Ma, respectively. Notably, the 2531 Ma granitic gneiss was identified for the first time in this region. Based on the geochemical characteristics, the granitoids can be divided into two types. The 2531 and 2027 Ma groups display I-type features, while the 2189–2173 and 1852 Ma groups exhibit A-type geochemical affinities. Both I-type groups exhibit enrichment in Rb, depletion in Nb, Ta, and Ti, moderate fractionated REE patterns, substantial negative Eu anomalies, low Sr/Y ratios, and positive $\varepsilon_{Hf}(t)$ (+3.51 to +5.53 and +5.59 to +7.32, respectively), indicating that they were generated from partial melting of the juvenile mafic crust. In contrast, the 2189–2173 Ma granitoids belong to A_2-type and were most likely generated by the partial melting of felsic rocks in the back-arc region, while the 1852 Ma granitoids belong to A_1-type and were most possibly the result of partial melting of mafic-intermediate rocks during the post-collisional stage. Based on the records of A-type granitic magmatism and the ~1950 Ma peak metamorphism throughout the Trans-North China Orogen, we propose that a long-lived subduction process (2531–1950 Ma) can mostly explain the existing geological phenomena. It is likely that the subduction between the Eastern and Western Blocks should have commenced at ~2531 Ma, followed by a long-lived subduction. The two blocks ultimately collided with each other to form the North China Craton at ~1950 Ma, which triggered post-collisional exhumation and partial melting at ~1852 Ma.

1. Introduction

The North China Craton (NCC) is considered to be one of the oldest cratons on the planet. Despite the wide acceptance of the tectonic division of the basement of the NCC into the Eastern and Western Blocks, separated by the intervening Trans-North China Orogen (TNCO) [1], the tectonic evolution of the NCC remains a considerable controversy among scholars (Figure 1). Several models have been proposed to explain the tectonic evolution of the NCC, including: (1) a prolonged subduction that lasted for ~650 Ma before the Eastern and Western Blocks finally collided at ~1850 Ma [2–6]; (2) a rift event that occurred after the amalgamation of the NCC at ~2500 Ma [7, 8]; (3) two stages of subduction–rift systems that occurred at 2450–2120 Ma and 2120–1980 Ma [9]; (4) two oceans

that formed by rifting at ~2300 Ma and that closed via subduction, successively, at ~2150 and ~1900–1860 Ma [10–13]; and (5) two microcontinents/oceanic plateaus that were accreted at ~2500 Ma, followed by a rift event and subduction polarity reversal [14–17]. Of these, the subduction polarity (eastward or westward) and whether there existed a vast ocean that lasted for ~650 Ma before the final collision remain the two major controversies.

In order to constrain the above issues, it is necessary to uncover the magmatism records from the Neoarchean to Paleoproterozoic era. Previous studies have revealed that the calc-alkaline granitoid and volcanic rocks in the Wutai greenstone belt represent the earliest evidence of arc-related magmatism in the TNCO at 2560–2520 Ma [18, 19]. Similarly aged 2560–2438 Ma granitoids have been recognized in other Terranes of the TNCO, including Xuanhua, Huai'an, Hengshan, Wutai, Fuping, Yunzhongshan, and Zhongtiao Complexes [2, 20–31]. Located in the westernmost margin of the TNCO (Figure 2), the Lüliang Complex represents the most viable area for constraining the above debates. Previous studies have indicated that the Lüliang Complex is primarily composed of Paleoproterozoic granitic plutons and meta-supracrustal rocks [24, 32–40]. In this study, we present a comprehensive analysis of the late Neoarchean to Paleoproterozoic granitoids within the Lüliang Complex, including whole-rock major and trace element compositions, secondary ion mass spectrometry (SIMS) zircon U–Pb geochronology, and in-situ zircon Hf–O isotopes. For the first time, we reported the Neoarchean magmatism in the Lüliang Complex. Combined with available petrological, metamorphic, and structural data, the results of this study led us to reconstruct an integrated accretionary process from Neoarchean to Paleoproterozoic for tectonic evolution of the TNCO and to provide new insights to further test the existing tectonic models of the NCC.

2. Geological Background and Petrography

The NCC is widely considered to be formed through the collision between the Eastern and Western Blocks along the linear structural TNCO (Figure 1 [1–5, 10, 11, 13, 21, 36, 37, 40–44]). The two blocks exhibit differences in lithology, geochemistry, structure, metamorphism, and geochronology, which have been summarized by Zhao et al. [5] and Kusky et al. [15]. The nearly north-south trending TNCO, also named the Central Orogenic Belt [41], is located in the central part of the NCC. There is a consensus that the TNCO represents a typical continent-to-continent collisional orogen: (1) low-grade supracrustal foreland basin deposits [12]; (2) structural characteristics of strike-slip ductile shear zones, large-scale thrusting and folding, transcurrent tectonics, sheath folds, and mineral lineation [4, 6, 11, 45, 46]; and (3) medium- to high-grade metamorphism, with clockwise *P*-*T* paths involving near-isothermal decompression [44, 47–61]. From north to south, the TNCO consists of different metamorphic terranes such as Chengde, Northern Hebei, Xuanhua, Huai'an, Hengshan, Wutai, Fuping, Lüliang, Zanhuang, Zhongtiao, Dengfeng, and Taihua Complexes (Figure 1 [24]). The dominant rock types are Neoarchean to Paleoproterozoic tonalitic-trondhjemitic-granodioritic (TTG) gneisses, meta-supracrustal rocks, syn- to post-tectonic granitoids, and ultramafic to mafic rocks [9]. Most of these rocks exhibit arc-related geochemical and isotopic characteristics [62].

The Lüliang Complex is situated at the western margin of the central part of the TNCO and is composed of Paleoproterozoic supracrustal rocks and Neoarchean to Paleoproterozoic granitoid plutons that experienced greenschist- to granulite-facies metamorphism (Figure 2 [24, 32, 33, 44, 49, 61]; this study). The meta-supracrustal rocks of the Lüliang Complex are primarily composed of graphite-bearing pelitic gneisses/schists, marbles, quartzites, phyllites, meta-basalts, sandstones, meta-conglomerates, and dolomites [10, 24, 33–35, 37, 40, 63–66]. Based on their stratigraphy from bottom to top, these rocks can be subdivided into the Jiehekou, Lüliang, and Yejishan/Heichashan Groups (Figure 2 [25, 65, 66]).

Zhao et al. [24] classified the granitoids that intruded into the supracrustal rocks into pre-tectonic gneisses, syn-tectonic gneissic granites, and post-tectonic granites. The pre-tectonic gneisses consist of the Yunzhongshan TTG gneisses, Gaijiazhuang gneisses, and Chijianling–Guandishan gneisses (Figure 2). The Yunzhongshan gneisses are predominantly exposed to the northeastern part of the Lüliang Complex and have undergone metamorphism to the upper amphibolite facies. The TTG, monzogranitic gneisses, and high-Mg mafic-ultramafic rocks in the Yunzhongshan area, formed at 2540–2500 Ma, are interpreted to have originated in an arc setting [24, 29, 67, 68]. Yunzhongshan gneisses are considered as comparable to the adjacent 2520–2475 Ma Hengshan and Fuping TTG gneisses [2, 22–24, 69]. The 2408–2364 Ma Gaijiazhuang gneisses are in tectonic contact with the Lüliang Group and are composed of coarse-grained porphyritic gneisses and monzonitic granite [24, 70]. The 2173–2199 Ma Chijianling–Guandishan gneisses are strongly deformed, metamorphosed, and widely distributed in the southern and western parts of the complex (Figure 2 [24, 32]). The syn-tectonic 1832 ± 11 Ma Huijiazhuang fine- to medium-grained, weakly gneissic to massive granite clearly intrudes the Chijianling–Guandishan gneisses and contains numerous xenoliths of the Chijianling–Guandishan gneisses [24]. The Huijiazhuang granite is contemporaneous with the 1950–1800 Ma metamorphism of the TNCO [24, 39, 44]. The post-tectonic granites in the Lüliang Complex, including the 1800 ± 7 Ma Luyashan coarse-grained charnockite, 1807 ± 10 Ma Luchaogou coarse-grained prophyritic granite, and 1798–1790 Ma Tangershang/Guandishan fine-grained granite, all of which exhibit a massive or structureless texture [24, 32]. While previous studies have roughly established a geochronological framework for the Lüliang Complex, there is still a lack of systematic analysis of geochemical and isotopic data and their connection to the specific tectonic settings.

In this study, we collected twelve granitic samples from the key granitoid intrusions throughout the Lüliang Complex (Figure 2). Four age groups of granitoids were

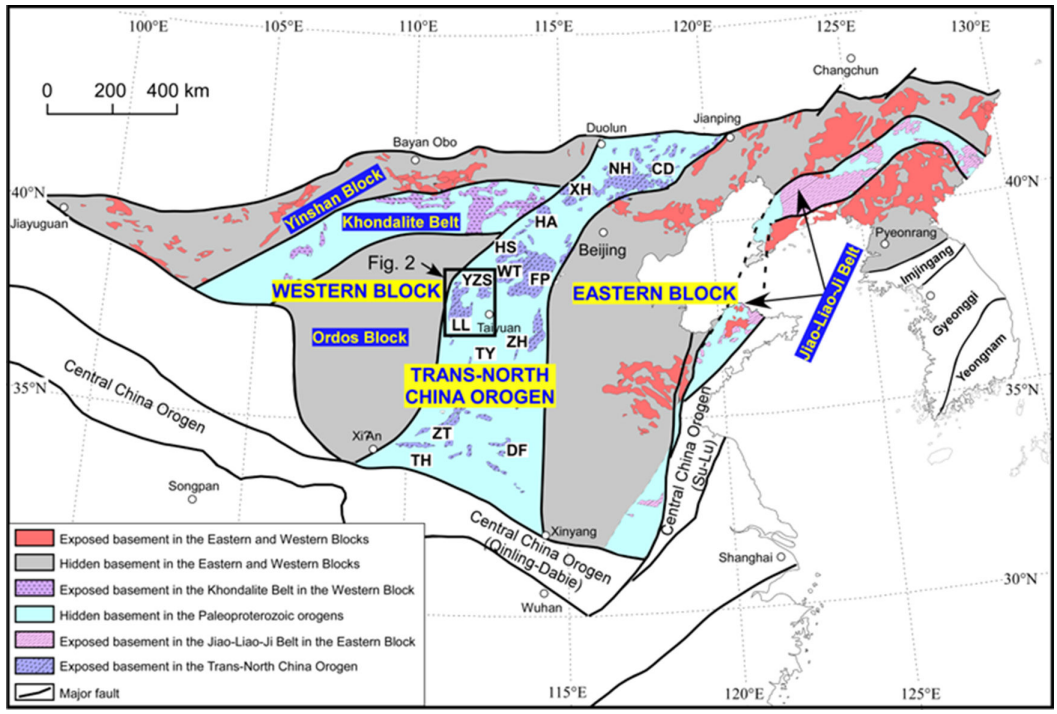

FIGURE 1: Tectonic subdivision of the NCC. Modified after Zhao et al. [123]. Abbreviations for metamorphic Complexes: CD, Chengde; DF, Dengfeng; FP, Fuping; HA, Huai'an; HS, Hengshan; LL, Lüliang; NH, Northern Hebei; TH, Taihua; TY, Taiyue; WT, Wutai; XH, Xuanhua; YZS, Yunzhongshan; ZH, Zanhuang; ZT, Zhongtiao.

identified based on our new SIMS data (see texts below; online supplementary Table S1). The first group is 2531 Ma granitic gneiss that was collected from the Fangshan County (Figure 2). In the field, the foliated granitic gneiss is truncated by undeformed granitic vein (Figure 3(a)). Microscopic observation indicates that the 2531 Ma granitic gneiss mainly consists of plagioclase (~30%), quartz (~25%), K-feldspar (~20%), and oriented mafic minerals including biotite (~15%) and hornblende (~5%), with a typical granitic texture and foliated structure (Figure 3(b)). The second group is 2189–2173 Ma deformed granite that was collected from the southwest area of the Lüliang Complex (Figure 2). This deformed granite shows penetrative foliation and the alignment of K-feldspar + plagioclase + biotite (Figure 3(c)). The representative mineral assemblage is K-feldspar (~30%), quartz (~25%), plagioclase (~25%), and biotite (~15%), displaying a granitic texture (Figure 3(d)). The third group is 2027 Ma granitic gneiss that was collected from an outcrop near the Wangjiagou primary school of Lüliang City (figures 2 and 3(e)). The rock is medium-grained and gneissic in structure and dominantly composed of K-feldspar (~30%), quartz (~25%), plagioclase (~25%), and oriented biotite (~15%), all of which exhibit a preferred alignment to form the major foliation (Figure 3(f)). The last group is 1852 Ma granite, which was collected from an abandoned quarry located ~1 km south of the main road in Kuaili Village, Xishe County (Figure 2). The rock is medium-grained and displays variation from strong strain domain of well-foliated texture to weak strain domain of massive structure (Figure 3(g)). The dominant mineral assemblage of this group is K-feldspar (~30%), quartz (~25%), plagioclase (~25%), and biotite (~15%), displaying a typical granitic texture (Figure 3(h)).

3. Analytical Methods and Results

Whole-rock major and trace element geochemistry, SIMS zircon U–Pb geochronology, and Hf–O isotope analyses were performed on representative granitic samples from the Lüliang Complex. The details of the analytical techniques are described in the online supplementary Text 1.

3.1. SIMS Zircon U–Pb Geochronology. Six representative samples were analyzed using zircon U–Pb dating. Four groups of granitoids with ages of 2531, 2189–2173, 2027, and 1852 Ma, respectively, were identified.

3.1.1. 2531 Ma Granitic Gneiss. Zircon grains from Sample 16LL35-1 are euhedral, appearing light brown to light orange and transparent. The crystals are commonly 100–250 μm in length, with length/width ratios of 1.5–2.0. Cathodoluminescence (CL) images from these zircon grains exhibit weak luminescence and display narrow bands of oscillatory zones, with no obvious core–rim textures and overgrowth rims, indicating a magmatic origin (Figure 4(a)). Eleven zircon grains were selected for SIMS U–Pb analyses, two of which were abandoned due to the excessive common Pb (online supplementary Table S1). The remaining nine analyses possess high Th/U ratios of 0.28–0.62. Seven analyses fall on the Concordant line and yield an apparent $^{207}Pb/^{206}Pb$ age between 2537 and 2515

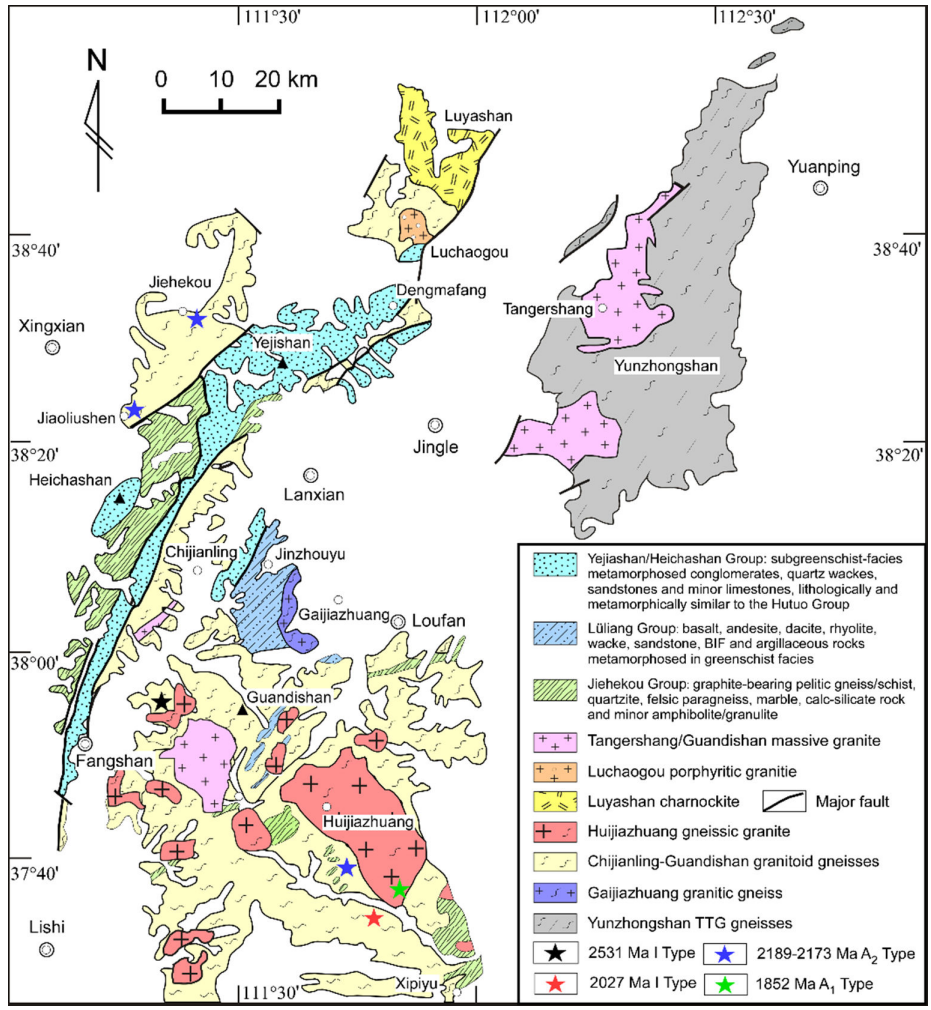

Figure 2: Geological map of the Lüliang Complex, modified after Zhao et al. [24].

Ma and a weighted mean $^{207}Pb/^{206}Pb$ age of 2531 ± 4 Ma (MSWD = 1.9, Figure 5(a)). This age can be interpreted as the crystallization age of this sample, and it is for the first time a Neoarchean age has been reported in the Lüliang Complex.

3.1.2. 2189–2173 Ma Deformed Granite. Three representative samples including 16LL26-2, 16LL31-1, and 16LL39-2 were dated using SIMS. Zircon grains from Sample 16LL26-2 are light gray to orange and transparent and have smaller sizes of 100–150 μm in length and length/width ratios of 1–2. Most grains are subhedral and show core–rim textures (Figure 4(b)). Wide bands of oscillatory zoning are generally preserved in the core section, and the rims show nebulous to "fir-tree" zoning (Figure 4(b) [71]). Some zircon grains show clear wide bands of oscillatory zonation surrounded by a thin rim (Figure 4(b)). Sixteen zircon grains with oscillatory zoning were selected for SIMS U–Pb analyses and display high Th/U ratios of 0.34–0.74 (online supplementary Table S1). Nine analyses fall on the Concordant line and yield an apparent $^{207}Pb/^{206}Pb$ age of 2194–2178 Ma with a weighted mean $^{207}Pb/^{206}Pb$ age of 2189 ± 5 Ma (MSWD = 2.4; Figure 5(b)). This age of 2189 ± 5 Ma can be interpreted to represent the crystallization age of the sample.

Zircon grains from Sample 16LL31-1 are subhedral, light gray to brown, and transparent to opaque. They are commonly 100–150 μm in length with length-to-width ratio of 1.5–2 (Figure 4(b)). They display oscillatory zoning cores and dark–thin metamorphic rims, though the rims are too narrow to analyze (Figure 4(b)). Twenty analyses of typical igneous zircon grains were conducted, of which eleven analyses with high Th/U ratios of 0.38–1.78 defined a discordant line with an upper intercept age of 2169 ± 10 Ma (MSWD = 0.9; Figure 5(c)). Five analyses falling on the Concordant line yield an apparent $^{207}Pb/^{206}Pb$ age of 2186–2161 Ma with a weighted mean $^{207}Pb/^{206}Pb$ age of 2173 ± 14 Ma (MSWD = 2.5, Figure 5(c)). It is indicated that the age of 2173 ± 14 Ma represents the crystallization age of the sample.

Zircon grains from Sample 16LL39-2 are euhedral and light red to brown. While they are mostly transparent, they contain some opacity caused by radiation damage, resulting in the transformation of the zircon from crystalline to an amorphous one. The zircon grains of this sample have lengths ranging from 100 to 200 μm with a length-to-width

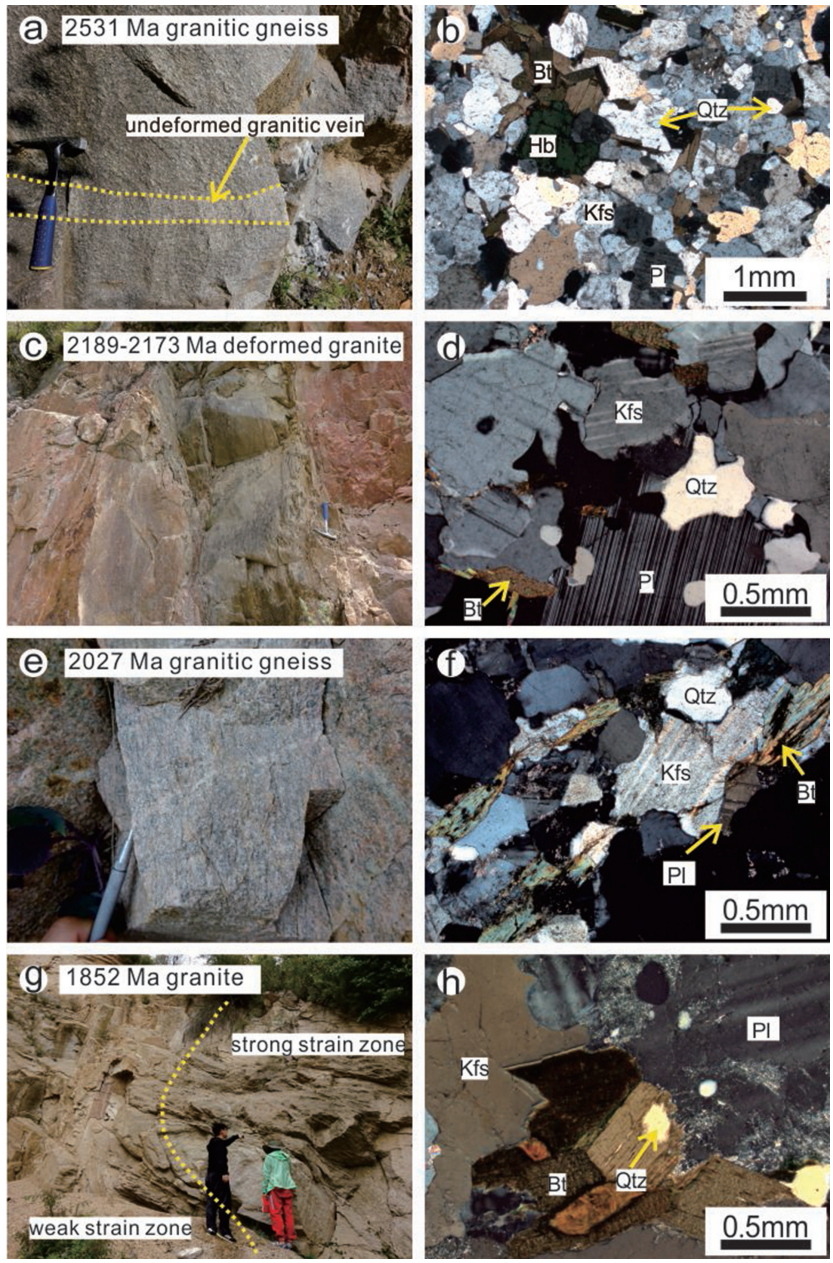

FIGURE 3: Representative field photographs (a, c, e, and g) and photomicrographs (b, d, f, and h) of the studied granitoids from the Lüliang Complex. Pl: plagioclase; Bt: biotite; Kfs: K-feldspar; Qtz: quartz; Hbl: hornblende.

ratios of ~2 (Figure 4(b)). The internal structure of the zircon grains is much more complicated, some of which show irregular internal structures, while some others still retain the oscillatory zonings (Figure 4(b)). Twenty-one spots on the oscillatory zoning areas were selected for U–Pb geochronological analyses. Nine available analyses exhibit high Th/U ratios of 0.20–0.74 and define a discordant line with an upper intercept age of 2178 ± 15 Ma (MSWD = 0.9; Figure 5(d)). The other four analyses on the Concordant line exhibit an apparent $^{207}Pb/^{206}Pb$ age of 2181–2163 Ma and yield a weighted mean $^{207}Pb/^{206}Pb$ age of 2175 ± 13 Ma (MSWD = 2.3; Figure 5(d)). In our interpretation, the age of 2175 ± 13 Ma can be regarded as the crystallization age of the sample.

3.1.3. 2027 Ma Granitic Gneiss. Zircon grains from Sample 16LL40-1 are light gray to brown, subhedral, and transparent to opaque. The zircon grain lengths are 150–200 μm, with a length-to-width ratio of ~2. In CL images, the opaque zircon grains show a spongy internal structure, and the translucent zircon grains still retain oscillatory zoning cores with bright and thin structureless rims (Figure 4(c)). Fourteen analyses on the oscillatory zoning areas were conducted, of which seven analyses display low common Pb, and high Th/U ratios (0.24, 0.53) were adopted and defined a discordant line with an upper intercept age of 2043 ± 21 Ma (MSWD = 0.4; Figure 5(e)). Three analyses on the Concordant line exhibit apparent $^{207}Pb/^{206}Pb$ age of 2035–2012 Ma and yield a weighted mean $^{207}Pb/^{206}Pb$ age of

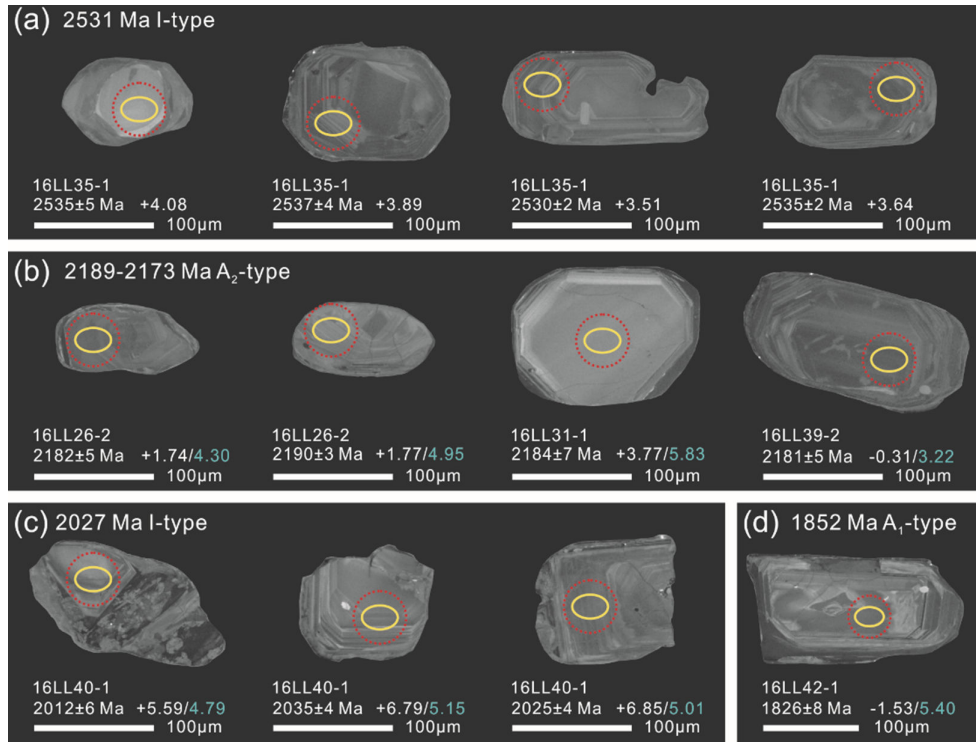

FIGURE 4: Representative CL images of zircon grains analyzed for in-situ U–Pb and Hf–O isotopes. The 20 × 30 μm yellow ellipse representing the SIMS analysis spots for U–Pb and O isotope, the 44 μm larger red circle representing the laser ablation multi-collector inductively coupled plasma mass spectrometry (LA-MC-ICPMS) analysis spots for Hf isotope. The data near the analysis spots are the $^{207}Pb/^{206}Pb$ age, $\varepsilon_{Hf}(t)$ value, and $\delta^{18}O$ value. The zircon grains are from (a) the 2531 Ma I-type granitic gneiss; (b) the 2189–2173 Ma A_2-type deformed granite; (c) the 2027 Ma I-type granitic gneiss; and (d) the 1852 Ma A_1-type granite.

2027 ± 25 Ma (MSWD = 5.3; Figure 5(e)). The age of 2027 ± 25 Ma can be interpreted as the crystallization age of this sample.

3.1.4. 1852 Ma Granite. Zircon grains of Sample 16LL42-1 are light yellow to light brown, euhedral, transparent, and partially opaque due to radiation damage. The zircon grains have lengths of 150–200 μm, with a length/width ratio of ~2. The CL images of the zircon grains are characterized by magmatic-origin oscillatory zoned cores with dark and structureless rims (Figure 4(d)). Twenty-two zircon grains were selected for U–Pb zircon analysis, of which ten analyses were discarded due to high common Pb contents (online supplementary Table S1). The remaining twelve analyses have high Th/U ratios of 0.09–1.62 and define a discordant line intersecting the Concordant line at 1852 ± 41 Ma (MSWD = 4.4; Figure 5(f)). One Concordant analysis yielded an apparent $^{207}Pb/^{206}Pb$ age of 1826 ± 8 Ma, which is consistent with the upper intercept age. The age of 1852 ± 41 Ma is regarded as the crystallization age. Zircon U–Pb age analyses are listed in online supplementary Table S1.

3.2. Whole-Rock Major and Trace Element Compositions. A total of twelve granitic samples were analyzed for whole-rock major and trace element geochemistry. They exhibit low loss on ignition (LOI) values of 0.34–1.07 wt%, suggesting a limited post-magmatic or metamorphic alteration (online supplementary Table S2). All the samples show relatively high SiO_2 values ranging from 70.27 to 76.91 wt%, variable $Fe_2O_3^T$ (1.37, 3.43 wt%) values, high K_2O (3.22, 6.37 wt%) and Na_2O (2.69, 4.29 wt%) contents, and high alkalis (K_2O+Na_2O = 7.19–9.60 wt%) but low CaO (0.50, 2.05 wt%) and MgO (0.22, 0.82 wt%, excluding one value of 2.40 wt%) values, and low $Mg^{\#}$ values (0.11, 0.38, excluding one value of 0.73; online supplementary Table S2). The studied granitoids yield Al_2O_3 contents of 11.80–14.46 wt% and A/CNK ($Al_2O_3/[CaO+Na_2O+K_2O]$ mol%) values of 1.04–1.10, defining a weakly peraluminous character (Figure 6(a)). The K_2O/Na_2O ratios range from 0.75 to 2.10. These granitoids also possess Rittman Index of 1.69–3.11 and plot in the high-K calc-alkaline field on the SiO_2 versus K_2O diagram (Figure 6(b)). On the TAS diagram, all samples fall within the granite region (Figure 6(c)).

On the primitive mantle-normalized spider diagram, all the studied samples are selective enrichment in large ion lithophile element (LILE) of Rb and depletion in high field strength elements (HFSE) of Nb, Ta, and Ti, marked negative Sr and Ba and positive Th, U, and Pb anomalies (Figure 7(a) and 7(c)). The total rare earth element (REE) contents of the 2531 and 2027 Ma age groups ranged from 156 to 283 ppm, which are lower than those of the 2189–2173 and 1852 Ma age groups that have total REE contents of 239–666 ppm (online supplementary Table S2). All the samples show fractionated right-declining chondrite-normalized REE patterns (Figure 7(b) and 7(d)).

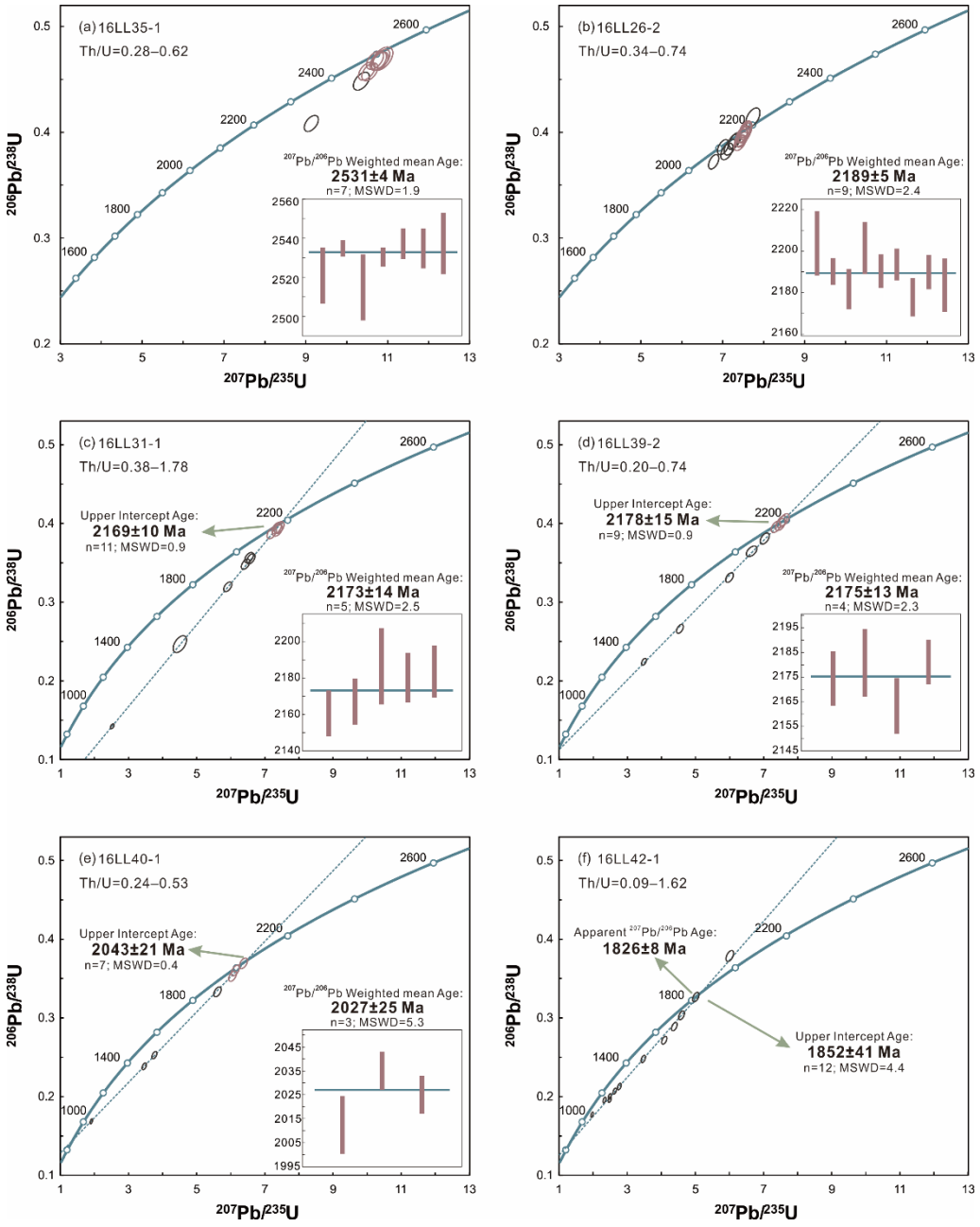

FIGURE 5: Concordia diagrams of SIMS U–Pb zircon analytical results for (a) the 2531 Ma I-type granitic gneiss, (b–d) the 2189–2173 Ma A_2-type deformed granite, (e) the 2027 Ma I-type granitic gneiss, and (f) the 1852 Ma A_1-type granite. MSWD: Mean Squared Weighted Deviates.

The three older groups (2531, 2189–2173, and 2027 Ma) are characterized by enrichments in light REEs with $(La/Yb)_N$ ratios of 7.01–70.14, relatively flat heavy rare earth elements (HREEs) with $(Gd/Yb)_N$ ratios of 0.86–7.28, and strong negative Eu anomalies ($Eu/Eu^* = 0.15–0.61$; Figure 7(b) and 7(d)). By contrast, the 1852 Ma age group shows significantly fractionated REE patterns, with $(La/Yb)_N$ ratios of 145.43–165.24 and $(Gd/Yb)_N$ ratios of 6.67–7.49, as well as moderate negative Eu anomalies ($Eu/Eu^* = 0.36–0.43$, Figure 7(d)). Whole-rock major and trace element compositions are listed in online supplementary Table S2.

3.3. Zircon Hf–O Isotope Compositions. The samples that were previously analyzed for U–Pb geochronology were further conducted for Hf isotope analysis (online supplementary Table S3). The crystallization ages were used to calculate the Hf two-stage model age (T_{DM}). The 2531 Ma age group yields homogeneous $^{176}Hf/^{177}Hf$ ratios of 0.281294–0.281357, corresponding to positive $\varepsilon_{Hf}(t)$ values of +3.51 to +5.53 and T_{DM} ages of 2656–2755 Ma (Figure 8). The 2189–2173 Ma age group shows a wide range of $^{176}Hf/^{177}Hf$ ratios between 0.281187 and 0.281554, mostly positive $\varepsilon_{Hf}(t)$ values of −0.31 to +3.76, except an outlier

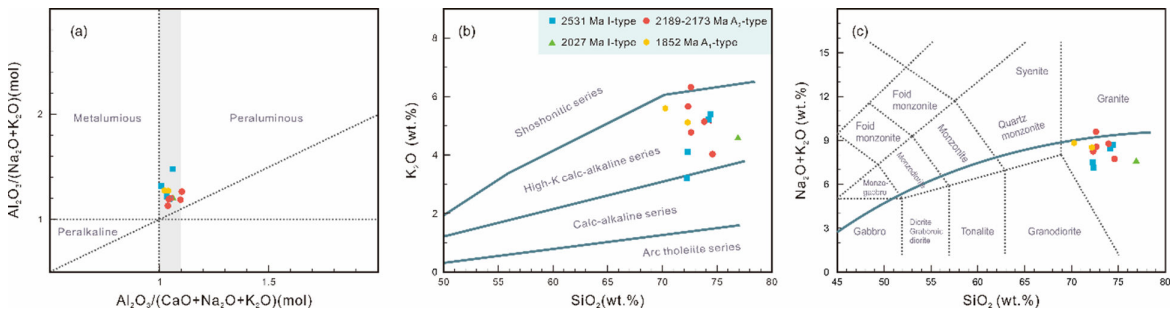

FIGURE 6: Geochemical classification diagrams for the studied granitoids from the Lüliang Complex: (a) A/NK versus A/CNK diagram [124]; (b) K_2O versus SiO_2 diagram [125]; (c) TAS diagram [126].

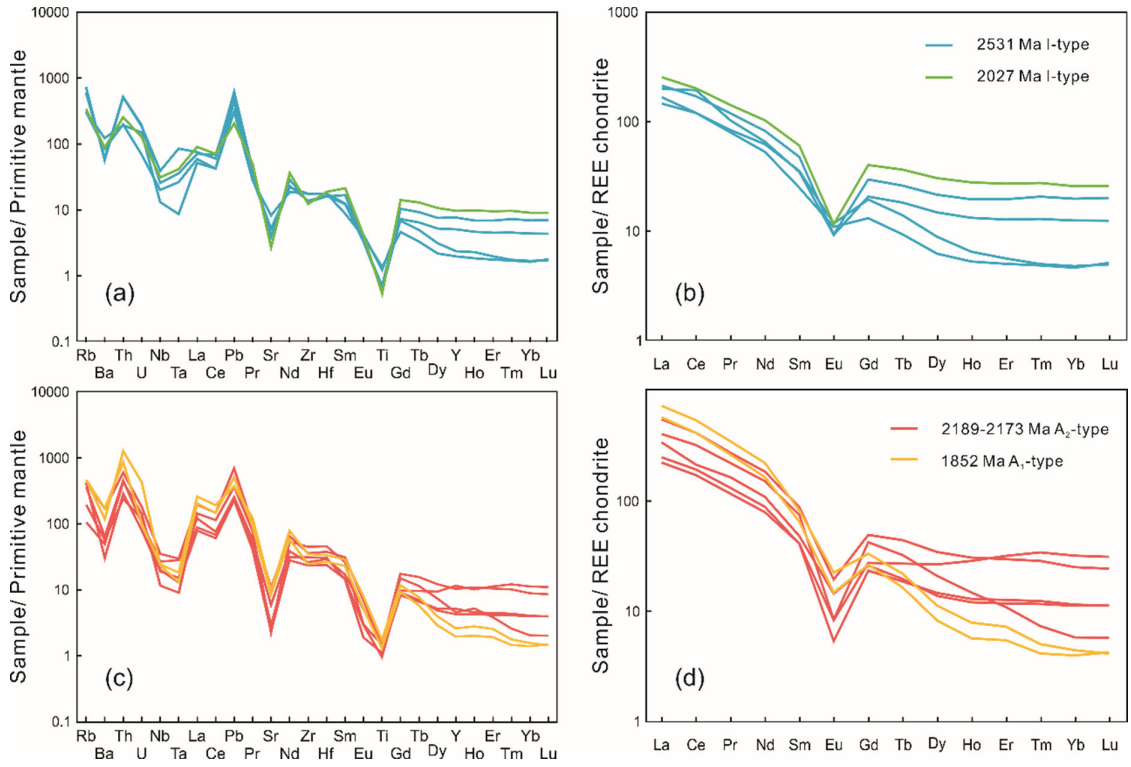

FIGURE 7: (a) Primitive mantle-normalized trace element diagrams and (b) chondrite-normalized REE diagrams of the studied granitoids from the Lüliang Complex. The normalization values are from Sun and McDonough [127].

with an $\varepsilon_{Hf}(t)$ of −8.37. This age group exhibits T_{DM} ages of 2450–2653 Ma (Figure 8). The 2027 Ma granitic gneiss exhibits concentrated positive $\varepsilon_{Hf}(t)$ values of +5.59 to +7.32, which are close to the depleted mantle line (Figure 8). This sample shows a narrow range of initial $^{176}Hf/^{177}Hf$ values of 0.281703–0.281762 and T_{DM} ages of 2154–2240 Ma (except for one outlier with an $\varepsilon_{Hf}[t]$ value of +4.63). The $\varepsilon_{Hf}(t)$ values of the 1852 Ma granite are below the chondrite evolution line and ranging from −4.98 to −1.53 (Figure 8). The scattered initial $^{176}Hf/^{177}Hf$ ratios of this group vary from 0.281482 to 0.281594, corresponding to the T_{DM} ages of 2451–2622 Ma and affinities to the 2189–2173 Ma deformed granite.

Five samples were subjected to in-situ SIMS oxygen isotope analysis (16LL26-2, 16LL31-1, 16LL39-2, 16LL40-1, and 16LL42-1). Analyses with U–Pb discordances >10% or high common Pb were excluded. The 2189–2173 Ma deformed granite has $\delta^{18}O$ values ranging from 3.22‰ to 6.31‰ (Figure 9), with an average of 5.21‰ ± 0.23‰ (n = 24; 2σ). The 2027 Ma granitic gneiss shows $\delta^{18}O$ values of 4.09‰–5.15‰ and an average of 4.76‰ ± 0.18‰ (n = 4, 2σ; Figure 9). The 1852 Ma granite has only two analyses near the Concordant line, displaying $\delta^{18}O$ values of 5.16‰–5.40‰ (Figure 9), with an average of 5.28‰ ± 0.24‰ (n = 2, 2σ). The zircon Hf–O isotope compositions are listed in online supplementary Tables S3 and S4.

4. Discussion

4.1. Classification of the 2531–1852 Ma Granitoids. The igneous rocks that have undergone strong alteration typically exhibit certain characteristics, such as high LOI

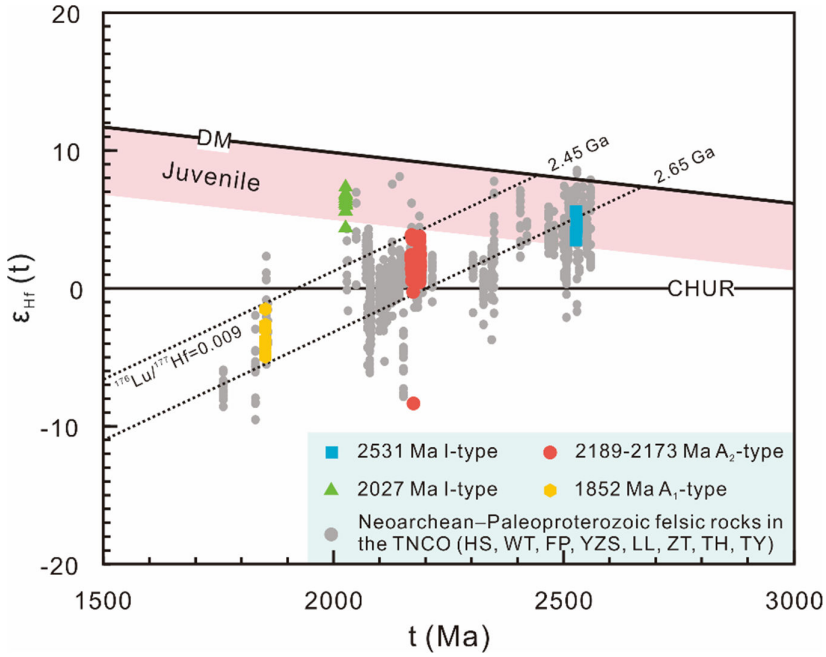

Figure 8: The $\varepsilon_{Hf}(t)$ values versus formation ages diagram of magmatic zircon grains from this study and the late Neoarchean to Paleoproterozoic felsic rocks in the TNCO [26, 27, 29, 38, 63, 109, 110, 112, 113, 118, 119, 128–137]. The depleted mantle evolution trend (DM) was constructed using the modern-day values of mid-ocean ridge basalts [138]. The corresponding lines of crustal extraction are calculated by assuming the $^{176}Lu/^{177}Hf$ ratio of 0.009 for the upper continental crust.

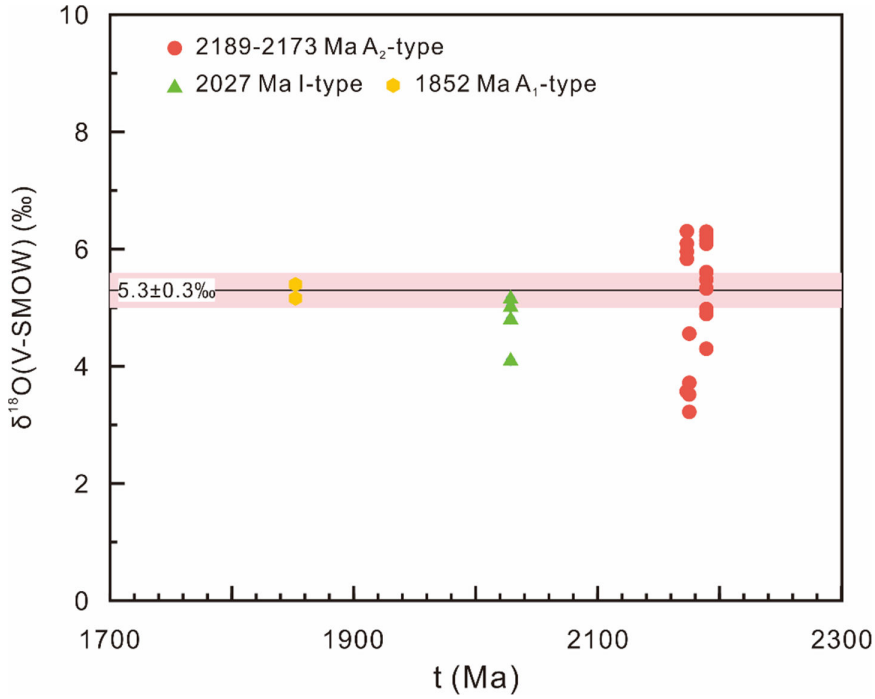

Figure 9: The $\delta^{18}O$ values versus formation ages for zircon analyses with U-Pb concordance >90% of the studied granitoids from the Lüliang Complex. The $\delta^{18}O$ value of mantle-like zircon grains is from Valley et al. [87].

values or significant Ce anomalies (|Ce/Ce*−1|>0.1 [72]). However, the studied samples show commonly low LOI values of 0.34–1.07 wt% and Ce/Ce* ratios of 0.90–1.35 (online supplementary Table S2), indicating weak alteration [72]. Chappell and White [73] proposed the classification for the protoliths of granitic rocks and divided them into two main groups: S-type (sedimentary) and I-type (igneous). Of the I-type group, Loiselle and Wones [74] introduced the A-type subgroup, which was further studied by Collins et al. [75]. The granitoids in this study can

be determined as I-type granites based on the following lines of evidence: (1) absence of Al-rich minerals, such as muscovite or magmatic garnet; (2) low A/CNK values (1.01, 1.10), indicating a weakly peraluminous characteristic (Figure 6(a)); (3) lower P_2O_5 (0.02, 0.11 wt%) and Al_2O_3 (11.80, 14.46 wt%) contents than typical S-type granite (Al_2O_3>14 wt%; online supplementary Table S2 [76, 77]); and (4) $\delta^{18}O$ values (<6.31‰) of magmatic zircon grains (Figure 9), indicating the involvement of limited sediments in the magma sources.

The primary components of granite are mainly influenced by the geochemical characteristics of its source region. Consequently, major elements are not effective in discriminating A-type granite from other types, particularly those with higher SiO_2 contents (>72% [78]). A high Ga/Al ratio has been utilized as a practical marker to distinguish A-type granite from other types [75]. All the studied granitoids display high 10,000*Ga/Al (>2.6) values in the A-type granite field (Figure 10a–10b). The Ga/Al ratio is most discernible for those strongly alkaline samples but less discernible for subalkaline samples [79]. This phenomenon can be attributed to the fact that the studied granitoids are felsic nonperalkaline, which may represent the highly fractionated I- or S-type granites [78, 79]. In addition, it is shown that the Ga/Al ratios of both I- and S-type granites tend to increase during the process of fractional crystallization, leading to comparable Ga/Al ratios as those observed in A-type granite [78]. Thus, the Zr+Nb+Ce+Y contents are more effective for differentiating highly fractionated S- or I-type granites from A-type granite [79]. As shown in Figure 10(c)–10(d), the 2189–2173 Ma deformed granite and 1852 Ma granite plot within the A-type field due to their high Zr+Nb+Ce+Y values, while the 2531 and 2027 Ma granitic gneisses overlap the area of fractionated felsic granites and unfractionated I- and S-type granites (OGT). This observation is consistent with the lower whole-rock Zr/Hf and Nb/Ta ratios of the 2531 and 2027 Ma granitic gneisses (Figure 10(e)). Moreover, fractional crystallization is a cooling process, as it progresses, the Ga/Al ratio of I- or S-type granites gradually increases, while the Zr content decreases and the Nb content increases; however, such correlations are not evident in A-type granite [78]. This trend is consistent with the negative correlation between Ga/Al and Zr and the positive correlation between Ga/Al and Nb observed in the 2531 and 2027 Ma granitic gneisses (Figure 10(a)–10(b)). Furthermore, the 2189–2173 Ma deformed granite and 1852 Ma granite exhibit higher calculated zircon saturation temperatures (845°C, 931°C) than those of the 2531 and 2027 Ma granitic gneisses (801°C, 826 °C; online supplementary Table S2). Additionally, the total REE contents of the 2189–2173 Ma deformed granite and 1852 Ma granite are significantly higher than those of the 2531 and 2027 Ma granitic gneisses (Figure 7, online supplementary Table S2). Therefore, it can be concluded that the 2189–2173 Ma deformed granite and 1852 Ma granite possess the characteristics of A-type granite, while the 2531 and 2027 Ma granitic gneisses display I-type features.

4.2. Petrogenesis of the 2531–1852 Ma Granitoids

4.2.1. 2531 Ma and 2027 Ma I-type Granitic Gneisses. As mentioned above, the 2531 and 2027 Ma granitic gneisses are I-type granites. And the I-type granite is thought to form through three possible mechanisms: (1) direct generation via fractional crystallization of mantle-derived basaltic magma [80]; (2) mixing of mantle-derived basaltic magma with crustal materials [81]; and (3) partial melting of mafic crustal rocks [82]. The granite that originated from extreme differentiation of mantle-derived magmas is usually found in association with a large amount of coeval mafic rocks and a series of igneous rocks with successive compositions from basaltic to granitic [83–85]. But such phenomena are absent in this region. Coeval (~2531 and ~2027 Ma) mafic magmatism is rare within the Lüliang Complex, except for an amphibolite with an upper intercept age of 2051 ± 68 Ma [66]. Thus, the possibility that the 2531 and 2027 Ma granitic gneisses were generated from fractional crystallization of mafic magma can be precluded. In addition, no petrologic or field evidence, for instance, component changes of minerals or micro-mafic enclaves within these granitoids support the magma mixing origin for the 2531 and 2027 Ma I-type granitic gneisses. Hf isotopic features are further opposed to the magma mixing origin because the 2531 and 2027 Ma I-type granitic gneisses exhibit homogeneous and positive $\varepsilon_{Hf}(t)$ values varying from +3.51 to +5.53 and +5.59 to +7.32 (Figure 8, online supplementary Table S3), respectively. Thus, partial melting of Neoarchean juvenile mafic crust might be the most likely mechanism for the 2531 and 2027 Ma I-type granitic gneisses of this study. The studied 2531 and 2027 Ma I-type granitic gneisses exhibit flat HREEs patterns, strong negative Eu anomalies (Figure 7(b)), lower Sr/Y ratios, and high Y values (Figure 10(f)). These features suggest a residue with abundant plagioclase with little or no garnet, which is indicative of melting at a shallow crustal level (<0.8 GPa or <30 km [86]). The 2027 I-type granitic gneiss displays low $\delta^{18}O$ values (4.79‰, 5.15‰; except for one value of 4.09‰ of the discordant analysis 40-1-11) within the range of mantle-like zircon grains (5.3‰ ± 0.3‰; Figure 9; online supplementary Table S4 [87]). O isotopes of the 2027 Ma I-type granitic gneiss suggest that the source region lacked significant recycled sediments or supracrustal rocks. In conclusion, the 2531 and 2027 Ma I-type granitic gneisses originated from the partial melting of juvenile mafic rocks at a relatively shallow crustal depth.

4.2.2. 2189–2173 Ma and 1852 Ma A-type Granites. Several petrogenetic models have been proposed for the origin of A-type granite, including (1) extreme differentiation of mantle-derived basaltic magma [88–91]; (2) partial melting of mafic–intermediate rocks in the middle–lower crust [92]; and (3) partial melting of felsic, infracrustal igneous rocks with H_2O contents similar to those of I-type granites in the shallow crust [78, 93, 94].

Mantle-derived A-type granite shares similarities with classic peralkaline A-type granite, which are identified by the presence of alkali minerals, such as amphibole,

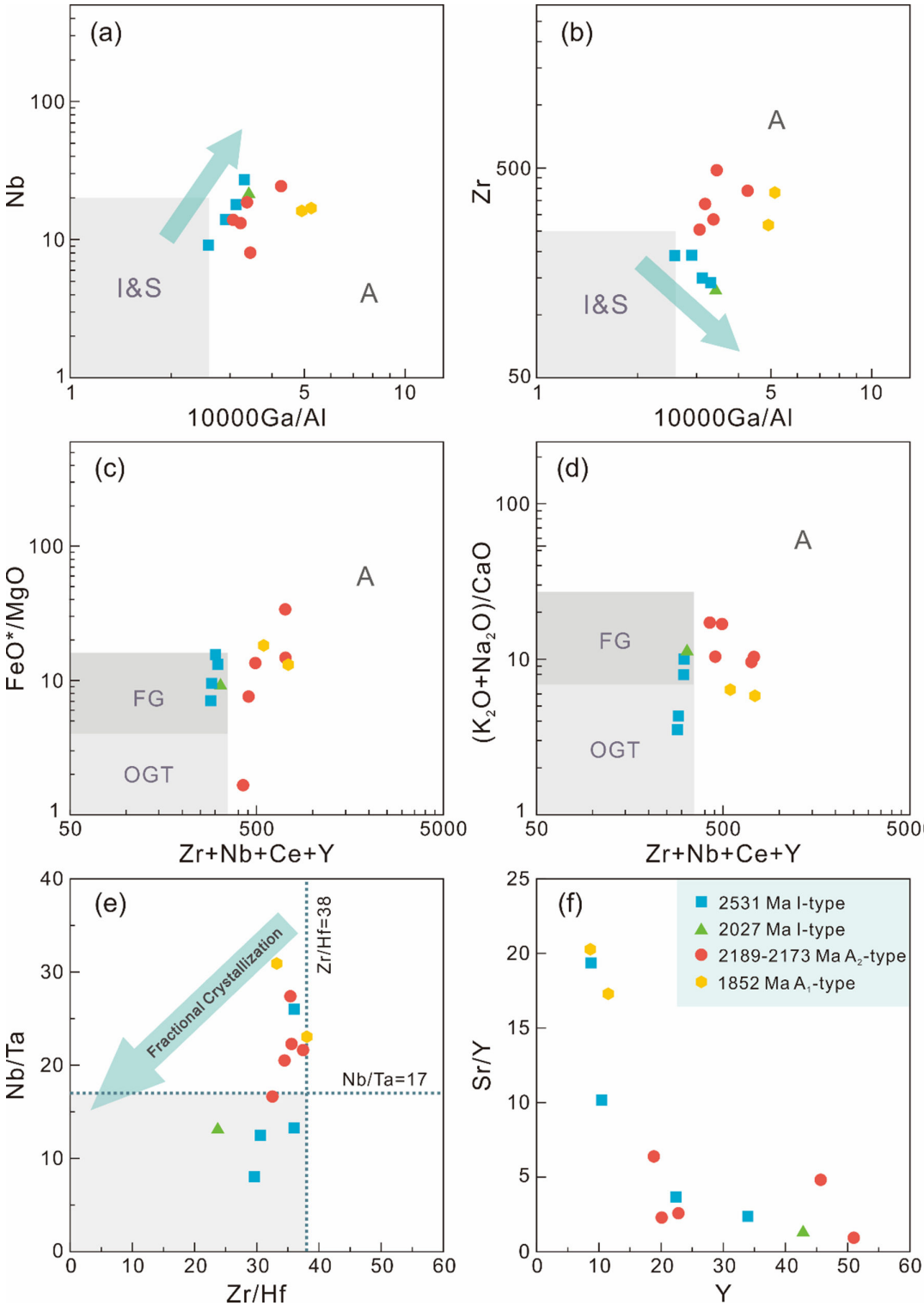

FIGURE 10: Plot of (a) 10000Ga/Al versus Nb; (b) 10000Ga/Al versus Zr; (c) Zr+Nb+Ce+Y versus FeO*/MgO; (d) Zr+Nb+Ce+Y versus $(K_2O+Na_2O)/CaO$; (e) Nb/Ta versus Zr/Hf; and (f) Sr/Y versus Y diagram. FG: fractionated felsic granites; OGT: unfractionated I- and S-type granites. The coordinates of these fields are: (a) $x = 2.6$, $y = 20$; (b) $x = 2.6$, $y = 250$; (c) $x = 350$, $y = 4$ and 16; (d) $x = 350$, $y = 7$ and 28 [79].

annite-rich biotite, and pyroxene, and often exhibit a narrow range of $\varepsilon_{Hf}(t)$ values that overlap or are slightly lower than those of the depleted mantle [75, 88, 91]. The 1852 Ma A-type granite displays extended negative $\varepsilon_{Hf}(t)$ values of −4.98 to −1.53 (online supplementary Table S3). The 2189–2173 Ma A-type deformed granite shows a wide

distribution of $\varepsilon_{Hf}(t)$ values, mostly positive ranging from +0.47 to +3.76 (except for two outliers of −0.31 and −8.37; Figure 8; online supplementary Table S3). However, these values remain significantly lower than those of the depleted mantle line. In addition, both the 2189–2173 Ma A-type deformed granite and 1852 Ma A-type granite yield A/CNK values of 1.02–1.10, A/NK values >1.13 and a lack of alkali mafic minerals, suggesting weakly peraluminous characteristics (Figure 6(a), online supplementary Table S2). The above features are inconsistent with mantle-derived A-type granite, ruling out the first mechanism.

Zircon grains from the 2189–2173 Ma A-type deformed granite display lower $\delta^{18}O$ values (3.22‰, 6.32‰) than mantle-like zircon grains (5.3‰ ± 0.3 ‰; Figure 9; online supplementary Table S4 [87]). This ^{18}O-depletion signature in zircon grains results from two possible mechanisms: (1) meteoric–hydrothermal alteration at high temperature [95, 96]; and (2) zircon crystallization from low-$\delta^{18}O$ magmas [97–100]. Given the slow rate of zircon growth and low oxygen diffusion rate [95, 101–103], it is unlikely for zircon to undergo isotopic re-equilibration during subsolidus (<600°C) meteoric–hydrothermal alteration within a geologically reasonable time frame [104–106]. The studied zircon grains with Concordant U–Pb ages yield low U contents (average of 304 ppm) and high Th/U ratios (0.29, 1.62, average of 0.66; online supplementary Table S1) and generally preserve typical oscillatory zonings in CL images (Figure 4), suggesting a magmatic origin and the absence of significant radiation damage or late alteration [107]. Therefore, the low-$\delta^{18}O$ signature of the 2189–2173 Ma A-type deformed granite is most likely inherited from their parental magma, which remelting of preexisting low-$\delta^{18}O$ materials (e.g., isotopic exchange between source rock and meteoric water/seawater at high temperature, namely, high-temperature water–rock reaction) rather than post-magmatic meteoric–hydrothermal alteration. The formation of A-type granite requires a high heat flow and extensional environment that increased fracture permeability. This allows surface water to reach the crustal depths of 8–10 km for deep hydrothermal circulation. This creates conditions favorable for generating low-$\delta^{18}O$ magmas [108]. These observations consequently imply that the source of the 2189–2173 Ma A-type deformed granite may have similar H_2O content as I-type granite. Furthermore, the 2189–2173 Ma A-type deformed granite exhibits moderate REE differentiation, substantial depletion of Eu (Figure 7(d)), decreased Sr/Y ratios, and elevated Y concentrations (Figure 10(f)), implying that they were formed through partial melting at a relatively shallow crust level (<0.8 GPa or <30 km). This is attributed to the absence of garnet but the presence of plagioclase in the residual source [86]. The major and trace element geochemistry, as well as the Hf–O isotopic signatures of the 2189–2173 Ma A-type deformed granite suggest a strong resemblance to A-type granite formed by partial melting of felsic igneous rocks with normal H_2O contents in the shallow crust.

Compared with the 2189–2173 Ma A-type deformed granite, the 1852 Ma A-type granite exhibits highly fractionated REE patterns, medium negative Eu anomalies (Figure 7(d)), and higher Sr/Y ratios with lower Y contents (Figure 10(f)), indicating the presence of residual garnet and plagioclase in the source. The presence of garnet further suggests that the partial melting occurred under pressures of 1.0–1.4 GPa or at a depth of 33–50 km in a slightly thickened crust [86]. The negative $\varepsilon_{Hf}(t)$ values of −4.98 to −1.53 indicate an ancient crust source for the 1852 Ma A-type granite. Thus, the 1852 Ma A-type granite was most likely derived from an ancient mafic–intermediate crust at the middle–lower crust.

4.3. Tectonic Process of the TNCO Before 1950 Ma. Multistage magmatic events were recorded in the Lüliang Complex, such as ~2410–2360 Ma Gaijiazhuang granitic gneiss [10, 11, 24, 109], ~2210–2100 Ma Chijianling–Guandishan granitoid gneisses [24, 32, 33, 35–38, 64, 110–112], ~2070–2020 Ma granitoid [32, 33, 38, 66, 111], and ~1870–1850 Ma Huijiazhuang gneissic granite. Most of these magmatic events are considered to have been generated in subduction-related environments [33, 111, 113]. As mentioned above, thus far, there has been no documentation of ~2500 Ma magmatism in the Lüliang Complex, with the sole exception of the Yunzhongshan TTG gneisses. The 2531 Ma I-type granitic gneiss from this study was first found and complement the mosaic geochronology in the Lüliang Complex. In addition, the 2531 Ma I-type granitic gneiss displays geochemical affinities to those originating from an arc setting. This is evidenced by their selected enrichment in Rb of LILE, depletion in Nb, Ta, and Ti of HFSEs, and fractionated REE patterns with negative Eu anomalies. Additionally, multiple terranes in the TNCO have recorded magmatic events during the Neoarchean period. For instance, the Datong-Huai'an Complex contains the TTGs emplaced at 2538–2497 Ma [25]; the Hengshan Complex contains the diorites, TTGs and volcanics with the age range of 2538–2483 Ma [26]; the Wutai Complex has granitoids with emplacement ages of 2560–2519 Ma [27]; the Fuping Complex has the TTG rocks emplaced at 2513 ± 13 Ma [28]. The Yunzhongshan area contains granitoid gneisses and metamorphosed volcano-sedimentary sequences formed at 2535–2486 Ma [29]; and the Zhongtiao Complex contains the Zhaizi and Xiyao TTGs formed at 2560–2536 Ma [30, 31]. All these granitoids are interpreted to have originated in tectonic settings associated with subduction-related environment, such as island arc, continental arc, or back-arc basin. Therefore, we suggest that a subduction-related regime is a more favorable interpretation for the geochemical and isotopic features of the 2531 Ma I-type granitic gneiss. The newly reported Neoarchean magmatism of the Lüliang Complex plays a pivotal role in bridging the northern and southern parts of the TNCO, establishing a new evidence chain of Neoarchean subduction system.

In recent years, more and more studies have reported the existence of Paleoproterozoic A-type granites in the TNCO. Some of the A-type granites are interpreted to have formed in a rift setting, and detailed information on these A-type granites in the TNCO

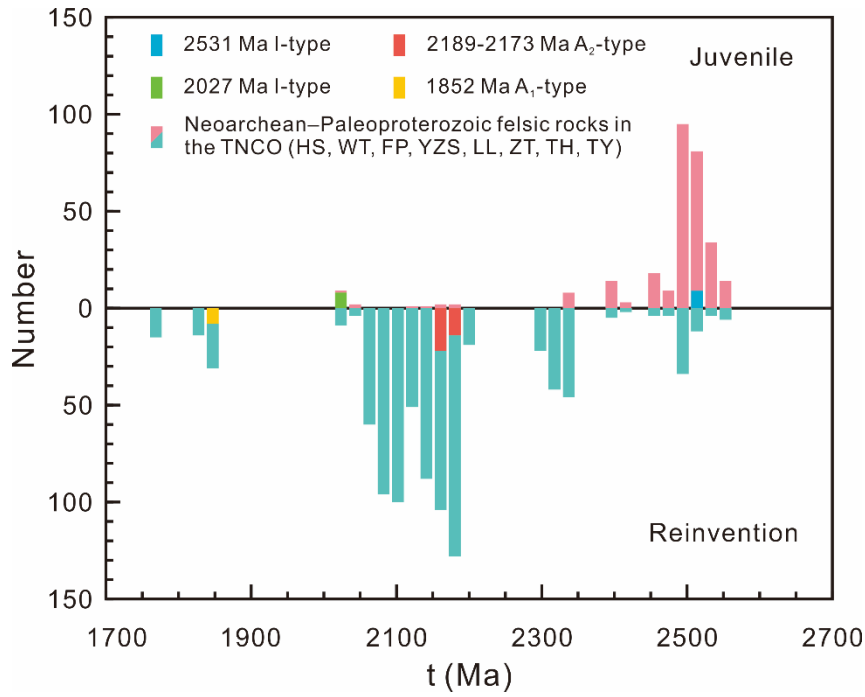

FIGURE 11: The number of magmatic zircon grains from this study and the Late Neoarchean to Paleoproterozoic felsic rocks in the TNCO, whose $\varepsilon_{Hf}(t)$ values overlap with and extend beyond the juvenile area, respectively [26, 27, 29, 38, 63, 109, 110, 112, 113, 118, 119, 128–137].

is summarized in Table 1. The generation of A-type granitic magma requires extensional decompression resulting from high heat flow, which can occur in different tectonic settings. These include within-plate rifting, post-orogenic delamination, and subduction [79, 114]. Therefore, a scheme involving a long-lived subduction–accretion system provides a clear explanation for the multistage A-type granitic magmatism throughout the tectonic evolution of the TNCO. The process of continental arc-related subduction involves a prolonged lithospheric extension, which is characterized by intermittent episodes of transient contraction [115]. During the extension phase, the retreat of the subducting slab triggers the lithospheric stretching, which leads to the decompression and melting of the asthenosphere. The upwelling asthenosphere beneath the back-arc region provides an external heat source for the formation of A-type granitic magma. The cycles of rapid alternation between contraction and lithospheric extension, also called tectonic switching, may document multiple episodes of A-type granitic magmatism and enhance efficient continental growth [115, 116]. In addition, Figure 8 presents a compilation of Hf isotopic and U–Pb chronological data for granitoids and equivalent felsic igneous rocks that were emplaced along the TNCO from the Neoarchean to Paleoproterozoic. The $\varepsilon_{Hf}(t)$ values that are close to or intersect with the depleted mantle line indicate that they were mostly derived from the partial melting of the juvenile crust [88]. Hf isotopic data further suggest the existence of juvenile crust or continental growth during the period of 2600–2000 Ma (Figure 11).

Eby [117] divided A-type granites into the A_1 and A_2 groups based on their Y/Nb ratios. The A_1 group is typically associated with continental rifts or intra-plate magmatism, whereas the A_2 group is believed to represent magma generated during continent–continent collision or island-arc processes [117]. The A-type granites identified in the TNCO predominantly exhibit A_2-type features prior to 1950 Ma, whereas the A_1-type signature became more prominent after 1950 Ma (Figure 12; Table 1). King et al. [78] proposed a further categorization of A-type granites into two subgroups (aluminous and peralkaline) based on the presence or absence of alkali mafic minerals. The aluminous group is derived from the partial melting of felsic crustal source rocks and has a similar H_2O content as I-type granite, while the peralkaline group is formed through the fractionation of mafic magma [78]. The studied 2189–2173 Ma A_2-type deformed granite, as well as others in the TNCO that were emplaced prior to 1950 Ma, exhibit metaluminous to peraluminous characteristics and fall into the aluminous A-type subgroup. This implies that the source of A-type granites was not affected by any substantial mantle-derived material, and the heat source mainly came from the asthenosphere. The low $\delta^{18}O$ signature observed in the 2189–2173 Ma A-type deformed granite suggests that they were derived from preexisting materials with low $\delta^{18}O$ values (Figure 9). This also implies that the TNCO during this period was not an entirely "anhydrous" environment.

The middle section of the TNCO comprises the Lüliang, Wutai, Fuping, and Zanhuang Complexes that align along a W-E-trending (Figure 1). The A-type

Table 1: Compilation of published A-type granites from the Trans-North China Orogen, North China Craton

Complex	Rock type	A_1/A_2	A/ACNK	Age	Reference
A-type granitoids emplaced before 1950 Ma					
Wutai	Granite porphyry	A_1–A_2	Peraluminous	Weighted mean $^{207}Pb/^{206}Pb$ age of 2137 ± 9 Ma	118
Fuping	Granitic gneiss	A_2	Metaluminous–peraluminous	Weighted mean $^{207}Pb/^{206}Pb$ ages of 2082–2063 Ma	119
Lüliang	Gneissic syenogranite	A_2	Peraluminous	Upper intercept ages of 2408–2398 Ma	109
Lüliang	Granitic gneiss	A_2	Metaluminous–peraluminous	Concordant ages of 2216–2110 Ma	110
Lüliang	Gioritic gneiss	A_2	Metaluminous–peraluminous	Concordant age of 2069 ± 5 Ma	110
Lüliang	Deformed granite	A_2	Peraluminous	Weighted mean $^{207}Pb/^{206}Pb$ ages of 2189–2173 Ma	This study
Lüliang	Feldspar porphyrite	A_2	Metaluminous–peraluminous	Weighted mean $^{207}Pb/^{206}Pb$ ages of 2189–2186 Ma	63
Zanhuang	Potassic and sodic granite	A_2	Metaluminous–peraluminous	Weighted mean $^{207}Pb/^{206}Pb$ ages of 2092–2066 Ma	120
Zanhuang	K-feldspar granite and monzonite	A_2	Metaluminous–peraluminous	Weighted mean $^{207}Pb/^{206}Pb$ age of 2090 ± 10 Ma	139
A-type granitoids emplaced after 1950 Ma					
Lüliang	Granite	A_1	Peraluminous	Upper intercept age of 1852 ± 41 Ma	This study
Lüliang	Porphyritic granite	A_2	Peraluminous	Weighted mean $^{207}Pb/^{206}Pb$ age of 1760 ± 20 Ma	113
Taihua	Granite	A_1	Metaluminous–peraluminous	Weighted mean $^{207}Pb/^{206}Pb$ ages of 1841–1800 Ma	140
Taihua	Granite	A_1–A_2	Metaluminous–peraluminous	Weighted mean $^{207}Pb/^{206}Pb$ ages of 1813–1789 Ma	141
Taihua	Granite	A_1	Metaluminous	Weighted mean $^{207}Pb/^{206}Pb$ age of 1830 ± 3 Ma	142
Taihua	Monzogranite	A_2	Metaluminous–peraluminous	Weighted mean $^{207}Pb/^{206}Pb$ ages of 1803–1797 Ma	143
Dengfeng	Granite	A_2	Metaluminous–peraluminous	Weighted mean $^{207}Pb/^{206}Pb$ ages of 1801–1795 Ma	144

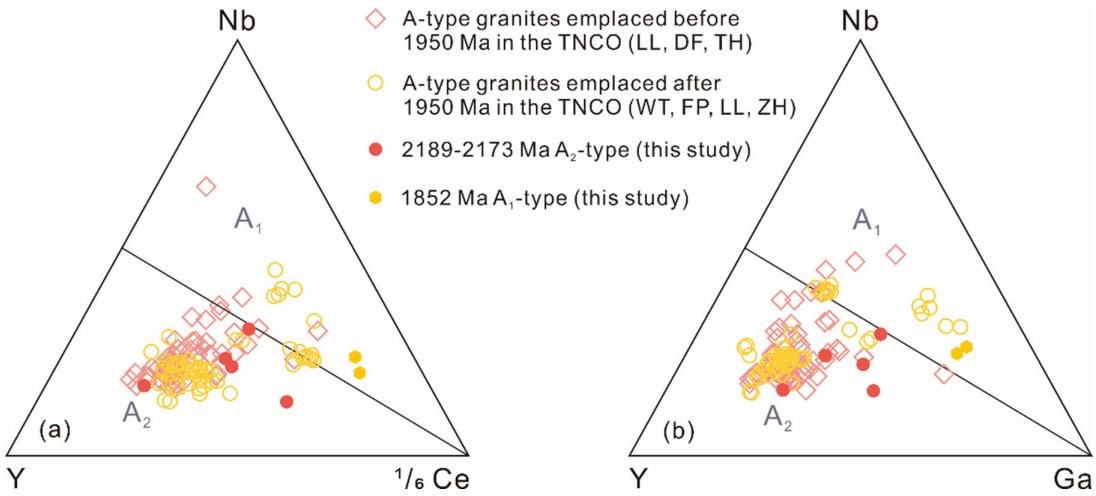

Figure 12: Comparison of the studied granitoids and the late Neoarchean to Paleoproterozoic A-type granites in the TNCO: (a) Y–Nb–1/6Ce; and (b) Y–Nb–Ga diagram of the A_1 and A_2 subgroups [117]. The geochemical dates of A-type granites are from Deng et al. [140, 143], Du et al. [63, 118, 120], Liu et al. [110], Mu et al. [141], Shi et al. [144], Wang et al. [119], Xue et al. [142], Yang et al. [139], and Zhao et al. [109, 113].

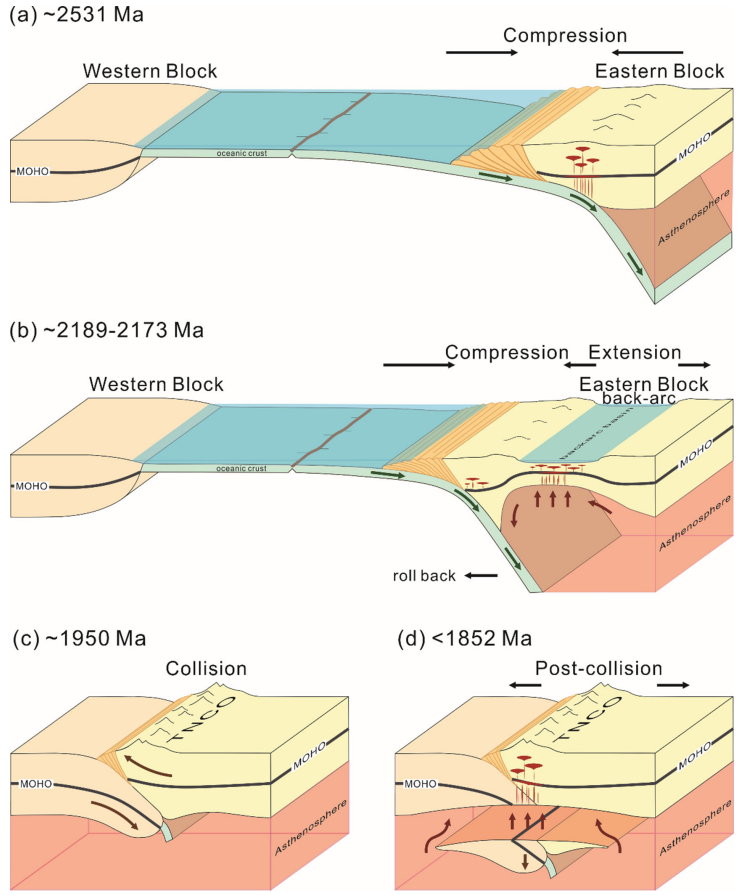

Figure 13: The model of the tectonic process between the Eastern and Western Blocks from late Neoarchean to Paleoproterozoic was conceptualized through the following stages (not to scale): (a) the early stage of the subduction between the Eastern and Western Blocks at ~2531 Ma; (b) regional extension induced by slab rollback, leading to asthenospheric upwelling and the formation of a back-arc basin at 2189–2173 Ma; (c) the peak stage of collision between the Eastern and Western Blocks at ~1950 Ma; (d) post-collisional extension resulting from the collapse of mountain roots at ~1852 Ma.

granites from these four complexes, which are of the same age, exhibit average zircon saturation temperatures of 879°C (this study; online supplementary Table S2), 884°C [118], 890°C [119], and 893°C [120], respectively. The gradual increase in crystallization temperature from west to east suggests that the Lüliang Complex is closer to the fore-arc region compared with other complexes. Moreover, the detrital zircon ages of metasedimentary rocks from the Lüliang Complex exhibit an age population of 2790–2600 Ma [37], while the xenolithic zircon ages from the Wutai Complex show an age population of 2763–2660 Ma [3], and the gneissic rocks from the Hengshan Complex represent old continental crustal components with an age range of 2712–2701 Ma [22]. These ages are in line with the 2700–2600 Ma crustal growth event in the Eastern Block as reported in previous studies [121, 122]. Therefore, we can infer that the Lüliang Complex was situated along the western margin of the Eastern Block, indicating the existence of eastward subduction of an ancient ocean between the Eastern and Western Blocks (Figure 13). In summary, we propose that the 2531–2027 Ma granitoids from the Lüliang Complex were formed in a magmatic arc environment, and the eastward subduction had already started at 2531 Ma.

4.4. Final Amalgamation of the NCC. It is widely believed that the collision between the Eastern and Western Blocks occurred at ~1950 Ma, which is supported by the numerous metamorphic zircon ages. For instance, granulite-facies metamorphism occurred at 1950–1920 Ma in the Lüliang Complex [44, 47, 49, 61] and is interpreted as the peak-stage metamorphism due to continental collision. Metamorphic ages of 1960–1950 and ~1920 Ma are also reported in the Hengshan Complex [50, 52, 55]. The former is interpreted as representing prograde or peak stages of metamorphism, while the latter indicates the cooling stages. In the Wutai area, prepeak or peak-stage metamorphism has been constrained at ~1950 Ma [50, 51]. The Huai'an Complex has a metamorphic history ranging from the HP granulite-facies stage of 1960–1900 Ma [58]. Decompression, external heat supply, and addition of hydrous fluid are the most significant factors influencing the formation of granite [114]. The available data from 1890–1800 Ma post-peak metamorphism and the clockwise near-isothermal decompression *P*–*T* path in the TNCO (e.g., Huai'an, Hengshan, Wutai, Fuping, Lüliang, and Taihua Complexes [44, 47–58, 60, 61]) support the idea that post-collisional extension and the associated asthenospheric upwelling were the mostly possible heat source that resulted in the formation of 1852 Ma A-type granite.

Based on the available data, we propose a tectonic scenario involving a long-lived subduction process for the tectonic evolution of the TNCO from late Neoarchean to Paleoproterozoic (Figure 13). At ~2531 Ma, an eastward subduction began in a vast ocean between the Eastern and Western Blocks and led to the formation of a continental arc along the western margin of the Eastern Block (Figure 13(a)). Following this, the subducting slab retreated, resulting in regional extension and the formation of back-arc basins at 2189–2173 Ma (Figure 13(b)). This long-lived subduction process involved several cycles of tectonic switching from slab subduction to roll-back, which effectively triggered multiple episodes of subduction-related magmatism and contributed to the generation of continental crust (Figure 13(b)). Finally, the collision between the Eastern and Western Blocks along the TNCO resulted in the peak-stage metamorphism at ~1950 Ma (Figure 13(c)). The collision persisted until the collapse of mountain roots, which triggered asthenospheric upwelling and post-collisional magmatism at ~1852 Ma (Figure 13(d)).

5. Conclusions

Four groups of granitoids have been recognized in the Lüliang Complex, including 2531 Ma I-type granitic gneiss, 2189–2173 Ma A_2-type deformed granite, 2027 Ma I-type granitic gneiss, and 1852 Ma A_1-type granite. The newly reported 2531 Ma I-type granitic gneiss represents the oldest known granitoid in the Lüliang Complex. This granitoid, along with the 2027 Ma I-type granitic gneiss, is thought to have originated from the partial melting of juvenile mafic crust in a magmatic arc environment. The 2189–2173 Ma A_2-type deformed granite was formed by partial melting of felsic igneous rocks in the shallow crust with normal H_2O content, which most likely developed at the back-arc basin. The 1852 Ma A_1-type granite was formed by partial melting of mafic–intermediate rocks in middle–lower crust at a post-collisional setting. The evolution of the Lüliang Complex is characterized by the eastward subduction of a vast ocean between the Eastern and Western Blocks, which started during the 2531 Ma and lasted until 1852 Ma. This prolonged period of subduction recorded multiple episodes of subduction-related magmatic events. The collision between the two Blocks occurred at ~1950 Ma to form the TNCO, resulting in the final amalgamation of the NCC.

Data Availability

The data that support the findings of this study are available from the published papers cited in the references list and included as supplementary material within the article.

Conflicts of Interest

The authors declare that there is no conflict of interest regarding this paper.

Acknowledgments

We are grateful to journal editors Prof. Tamer S. Abu-Alum and Prof. Songjian Ao, as well as two anonymous reviewers for their constructive comments that helped us improve the manuscript. We would like to thank Qing Yang, Wanfeng Zhang, and Boqin Xiong for their assistance during the SIMS U–Pb geochronology and O isotopic analyses.

This study is financially supported by the Natural Science Foundation of China (42025204, 41890381, 42202225, and 41972197).

Supplementary Materials

Supplementary Text 1: analytical techniques. Supplementary Table 1: zircon SIMS Th–U–Pb data of the granitoids from the Lüliang Complex, North China Craton. Supplementary Table 2: major and trace element geochemistry of the granitoids from the Lüliang Complex, North China Craton. Supplementary Table 3: zircon in-situ LA-ICPMS-MC Lu–Hf isotopic data of the granitoids from the Lüliang Complex, North China Craton. Supplementary Table 4: zircon in-situ SIMS O isotopic data of the granitoids from the Lüliang Complex, North China Craton.

References

[1] G. C. Zhao, P. A. Cawood, S. A. Wilde, M. Sun, and L. Z. Lu, "Metamorphism of basement rocks in the central zone of the North China Craton: implications for Paleoproterozoic Tectonic evolution," *Precambrian Research*, vol. 103, nos. 1–2, pp. 55–88, 2000.

[2] A. Kröner, S. A. Wilde, G. C. Zhao, et al., "Zircon Geochronology of Mafic Dykes in the Hengshan complex of northern China: evidence for late Palaeoproterozoic Rifting and subsequent high-pressure event in the North China Craton, " *Precambrian Research*, vol. 146, nos. 1–2, pp. 45–67, 2006.

[3] S. A. Wilde, G. C. Zhao, and M. Sun, "Development of the North China Craton during the late Archaean and its final amalgamation at 1.8 Ga: some speculations on its position within a global Palaeoproterozoic Supercontinent," *Gondwana Research*, vol. 5, no. 1, pp. 85–94, 2002.

[4] J. Zhang, G. C. Zhao, S. Z. Li, et al., "Deformation history of the Hengshan complex: implications for the Tectonic evolution of the Trans-North China Orogen," *Journal of Structural Geology*, vol. 29, no. 6, pp. 933–949, 2007.

[5] G. C. Zhao, S. A. Wilde, P. A. Cawood, and M. Sun, "Archean blocks and their boundaries in the North China Craton: Lithological, Geochemical, structural and P–t, path constraints and Tectonic evolution," *Precambrian Research*, vol. 107, nos. 1–2, pp. 45–73, 2001.

[6] J. Zhang, G. C. Zhao, S. Z. Li, M. Sun, and S. W. Liu, "Structural and Aeromagnetic studies of the Wutai complex: implications for the Tectonic evolution of the Trans-North China Orogen," *Precambrian Research*, vols. 222–223, pp. 212–229, 2012.

[7] M. G. Zhai, "Multi-stage Crustal growth and Cratonization of the North China Craton," *Geoscience Frontiers*, vol. 5, no. 4, pp. 457–469, 2014.

[8] M. G. Zhai, T. S. Li, P. Peng, et al., "Precambrian key Tectonic events and evolution of the North China Craton," *Geological Society, London, Special Publications*, vol. 338, no. 1, pp. 235–262, 2010.

[9] L. Tang and M. Santosh, "Neoarchean–Paleoproterozoic Terrane assembly and Wilson cycle in the North China Craton: an overview from the central segment of the Trans-North China Orogen," *Earth-Science Reviews*, vol. 182, pp. 1–27, 2018.

[10] M. Faure, P. Trap, W. Lin, P. Monié, and O. Bruguier, "Polyorogenic evolution of the Paleoproterozoic Trans-North China belt, new insights from the Lüliangshan–Hengshan–Wutaishan and Fuping massifs," *Episodes*, vol. 30, no. 2, pp. 96–107, 2007.

[11] P. Trap, M. Faure, W. Lin, and P. Monié, "Late Paleoproterozoic (1900–1800 ma) Nappe stacking and Polyphase deformation in the Hengshan–Wutaishan area: implications for the understanding of the Trans-North China belt, North China Craton," *Precambrian Research*, vol. 156, nos. 1–2, pp. 85–106, 2007.

[12] P. Trap, M. Faure, W. Lin, and S. Meffre, "The Lüliang Massif: a key area for the understanding of the Palaeoproterozoic Trans-North China belt, North China Craton," *Geological Society, London, Special Publications*, vol. 323, no. 1, pp. 99–125, 2009.

[13] P. Trap, M. Faure, W. Lin, N. Le Breton, and P. Monié, "The Paleoproterozoic evolution of the Trans-North China Orogen: toward a synthetic Tectonic model," *Precambrian Research*, vols. 222–223, pp. 191–211, 2012.

[14] H. Deng, T. M. Kusky, A. Polat, et al., "A 2.5 Ga fore-arc Subduction-accretion complex in the Dengfeng granite-Greenstone belt, Southern North China Craton," *Precambrian Research*, vol. 275, pp. 241–264, 2016.

[15] T. M. Kusky, A. Polat, B. F. Windley, et al., "Insights into the Tectonic evolution of the North China Craton through comparative Tectonic analysis: a record of outward growth of Precambrian continents," *Earth-Science Reviews*, vol. 162, pp. 387–432, 2016.

[16] J. P. Wang, T. M. Kusky, L. Wang, A. Polat, and H. Deng, "A Neoarchean Subduction polarity reversal event in the North China Craton," *Lithos*, vols. 220–223, pp. 133–146, 2015.

[17] J. P. Wang, T. M. Kusky, L. Wang, et al., "Structural relationships along a Neoarchean arc–continent collision zone, North China Craton," *Acta Geologica Sinica - English Edition*, vol. 90, no. s1, pp. 242–243, 2016. https://onlinelibrary.wiley.com/toc/17556724/90/s1.

[18] S. A. Wilde, P. A. Cawood, K. Y. Wang, A. Nemchin, and G. C. Zhao, "Determining Precambrian Crustal evolution in China: a case-study from Wutaishan, Shanxi province, demonstrating the application of precise SHRIMP U–PB Geochronology," *Geological Society, London, Special Publications*, vol. 226, no. 1, pp. 5–25, 2004.

[19] S. A. Wilde, P. A. Cawood, K. Wang, and A. A. Nemchin, "Granitoid evolution in the late Archean Wutai complex, North China Craton," *Journal of Asian Earth Sciences*, vol. 24, no. 5, pp. 597–613, 2005.

[20] H. Guan, M. Sun, S. A. Wilde, X. H. Zhou, and M. G. Zhai, "SHRIMP U–PB Zircon Geochronology of the Fuping complex: implications for formation and assembly of the North China Craton," *Precambrian Research*, vol. 113, nos. 1–2, pp. 1–18, 2002.

[21] J. H. Guo, M. Sun, F. K. Chen, and M. G. Zhai, "Sm–nd and SHRIMP U–PB Zircon Geochronology of high-pressure Granulites in the Sanggan area, North China Craton: timing of Paleoproterozoic Continental collision," *Journal of Asian Earth Sciences*, vol. 24, no. 5, pp. 629–642, 2005.

[22] A. Kröner, S. A. Wilde, J. H. Li, and K. Y. Wang, "Age and evolution of a late Archaean to early Palaeozoic upper to lower Crustal section in the Wutaishan/Hengshan/Fuping terrain of northern China," *Journal of Asian Earth Sciences*, vol. 24, no. 5, pp. 577–595, 2005.

[23] G. C. Zhao, S. A. Wilde, P. A. Cawood, and M. Sun, "SHRIMP U–PB Zircon ages of the Fuping complex: implications for late Archean to Paleoproterozoic accretion and assembly of the North China Craton," *American Journal of Science*, vol. 302, no. 3, pp. 191–226, 2002.

[24] G. C. Zhao, S. A. Wilde, M. Sun, S. Z. Li, X. P. Li, and J. Zhang, "SHRIMP U–PB Zircon ages of Granitoid rocks in the Luliang complex: implications for the accretion and evolution of the Trans-North China Orogen," *Precambrian Research*, vol. 160, nos. 3–4, pp. 213–226, 2008.

[25] Y. Chen, J. Zhang, P. Gao, et al., "Modern-style plate Tectonics manifested by the late Neoarchean TTG-Sanukitoid suite from the Datong-Huai'An complex, Trans-North China Orogen," *Lithos*, vols. 430–431, p. 106843, 2022.

[26] Y. L. Hu, S. W. Liu, J. H. Fu, G. Z. Sun, L. Gao, and R. R. Guo, "Neoarchean–early Paleoproterozoic Granitoids, the geothermal gradient and Geodynamic evolution in the Hengshan Terrane," *Gondwana Research*, vol. 94, pp. 143–163, 2021.

[27] D. Sun, Q. G. Li, S. W. Liu, et al., "Neoarchean–Paleoproterozoic Magmatic arc evolution in the Wutai–Hengshan–Fuping area, North China Craton: new perspectives from Zircon U–PB ages and HF isotopic data," *Precambrian Research*, vol. 331, 2019.

[28] L. Tang, M. Santosh, T. Tsunogae, and X. M. Teng, "Late Neoarchean arc Magmatism and Crustal growth associated with Microblock amalgamation in the North China Craton: evidence from the Fuping complex," *Lithos*, vols. 248–251, pp. 324–338, 2016.

[29] X. Wang, Y. F. Zheng, and W. B. Zhu, "Geochemical evidence for Reworking of the juvenile crust in the Neoarchean for Felsic Magmatism in the Yunzhongshan area, the North China Craton," *Precambrian Research*, vol. 335, 2019.

[30] L. S. Guo, S. W. Liu, Y. L. Liu, et al., "Zircon HF isotopic features of TTG Gneissed and formation environment of Precambrian Sushui complex in Zhongtiao mountains," *Acta Petrologica Sinica*, vol. 24, pp. 139–148, 2008.

[31] T. Wei, L. Shuwen, L. Chaohui, Y. Shengqiang, L. Qiugen, and W. Yueran, "Zircon SHRIMP Geochronology and geochemistry of TTG rocks in Sushui complex from Zhongtiao mountains with its geological implications," *Progress in Natural Science*, vol. 16, no. 5, pp. 492–500, 2006.

[32] Y. S. Geng, Y. S. Wan, Q. H. Shen, H. M. Li, and R. X. Zhang, "Chronological framework of the early Precambrian important events in the Lüliang area, Shanxi province," *Acta Geologica Sinica*, vol. 74, no. 3, pp. 216–223, 2000.

[33] S. Liu, Q. Li, C. Liu, Y. Lü, and F. Zhang, "Guandishan Granitoids of the Paleoproterozoic Lüliang metamorphic complex in the Trans-North China Orogen: SHRIMP Zircon ages, Petrogenesis and Tectonic implications," *Acta Geologica Sinica - English Edition*, vol. 83, no. 3, pp. 580–602, 2009.

[34] C. Liu, G. Zhao, M. Sun, et al., "U–PB and HF isotopic study of Detrital Zircons from the Yejishan group of the Lüliang complex: constraints on the timing of collision between the Eastern and Western blocks, North China Craton," *Sedimentary Geology*, vol. 236, nos. 1–2, pp. 129–140, 2011.

[35] C. H. Liu, G. C. Zhao, F. L. Liu, M. Sun, J. Zhang, and C. Q. Yin, "Zircons U–PB and LU–HF isotopic and whole-rock Geochemical constraints on the Gantaohe group in the Zanhuang complex: implications for the Tectonic evolution of the Trans-North China Orogen," *Lithos*, vols. 146–147, pp. 80–92, 2012.

[36] C. Liu, G. Zhao, F. Liu, and J. Shi, "2.2 Ga Magnesian Andesites, Nb-enriched Basalt–Andesites, and Adakitic rocks in the Lüliang complex: evidence for early Paleoproterozoic Subduction in the North China Craton," *Lithos*, vols. 208–209, pp. 104–117, 2014.

[37] C. Liu, G. Zhao, F. Liu, and J. Shi, "Geochronological and Geochemical constraints on the Lüliang group in the Lüliang complex: implications for the Tectonic evolution of the Trans-North China Orogen," *Lithos*, vols. 198–199, pp. 298–315, 2014.

[38] M. Santosh, Q. Y. Yang, X. M. Teng, and L. Tang, "Paleoproterozoic Crustal growth in the North China Craton: evidence from the Lüliang complex," *Precambrian Research*, vol. 263, pp. 197–231, 2015.

[39] Y. S. Wan, Y. S. Geng, Q. H. Shen, and R. X. Zhang, "Khondalite series-Geochronology and geochemistry of the Jiehekou group in the Lüliang area, Shanxi province," *Acta Petrologica Sinica*, vol. 16, no. 1, pp. 49–58, 2000.

[40] X. P. Xia, M. Sun, G. C. Zhao, F. Y. Wu, and L. W. Xie, "U–PB and HF isotopic study of Detrital Zircons from the Lüliang Khondalite, North China Craton, and their Tectonic implications," *Geological Magazine*, vol. 146, no. 5, pp. 701–716, 2009.

[41] T. M. Kusky and J. H. Li, "Paleoproterozoic Tectonic evolution of the North China Craton," *Journal of Asian Earth Sciences*, vol. 22, no. 4, pp. 383–397, 2003.

[42] J. H. Li and T. M. Kusky, "A late Archean foreland fold and thrust belt in the North China Craton: implications for early Collisional Tectonics," *Gondwana Research*, vol. 12, nos. 1–2, pp. 47–66, 2007.

[43] M. Santosh, "Assembling North China Craton within the Columbia Supercontinent: the role of double-sided Subduction," *Precambrian Research*, vol. 178, nos. 1–4, pp. 149–167, 2010.

[44] L. L. Xiao, G. Clarke, F. L. Liu, and C. M. Wu, "Discovery of Mafic Granulite in the Guandishan area of the Lüliang complex, North China Craton: age and metamorphic evolution," *Precambrian Research*, vol. 303, pp. 604–625, 2017.

[45] S. Li, G. Zhao, S. A. Wilde, et al., "Deformational history of the Hengshan–Wutai–Fuping belt: implications for the evolution of the Trans-North China Orogen," *Gondwana Research*, vol. 18, no. 4, pp. 611–631, 2010.

[46] J. Zhang, G. C. Zhao, S. Z. Li, M. Sun, S. W. Liu, and C. Q. Yin, "Deformational history of the Fuping complex and new U–th–PB Geochronological constraints: implications for the Tectonic evolution of the Trans-North China Orogen," *Journal of Structural Geology*, vol. 31, no. 2, pp. 177–193, 2009.

[47] C. Liu, G. Zhao, F. Liu, W. Xu, and L. Zou, "The timing of Crustal thickening constrained by metamorphic Zircon U–PB–HF and trace element signatures in the Lüliang

complex, Trans-North China Orogen," *Precambrian Research*, vol. 367, 2021.

[48] J. H. Liu, Q. W. L. Zhang, Z. M. G. Li, H. C. G. Zhang, Y. C. Chen, and C. M. Wu, "Metamorphic evolution and U–PB Geochronology of Metapelite, northeastern Wutai complex: implications for Paleoproterozoic Tectonic evolution of the Trans-North China Orogen," *Precambrian Research*, vol. 350, 2020.

[49] C. Lu, J. Qian, C. Yin, P. Gao, M. Guo, and W. Zhang, "Ultrahigh temperature Metamorphism recorded in the Lüliang complex, Trans-North China Orogen: P–T–t evolution and heating mechanism," *Precambrian Research*, vol. 383, 2022.

[50] J. H. Qian and C. J. Wei, "P–T–t evolution of garnet Amphibolites in the Wutai–Hengshan area, North China Craton: insights from phase Equilibria and Geochronology," *Journal of Metamorphic Geology*, vol. 34, no. 5, pp. 423–446, 2016. https://onlinelibrary.wiley.com/toc/15251314/34/5.

[51] J. H. Qian, C. J. Wei, X. W. Zhou, and Y. H. Zhang, "Metamorphic P–T paths and new Zircon U–PB ages for garnet-mica Schist from the Wutai group, North China Craton," *Precambrian Research*, vol. 233, pp. 282–296, 2013.

[52] J. Qian, C. Wei, G. L. Clarke, and X. Zhou, "Metamorphic evolution and Zircon ages of garnet-Orthoamphibole rocks in Southern Hengshan, North China Craton: insights into the regional Paleoproterozoic P–T–t history," *Precambrian Research*, vol. 256, pp. 223–240, 2015.

[53] J. H. Qian, C. J. Wei, and C. Q. Yin, "Paleoproterozoic P–T–t evolution in the Hengshan–Wutai–Fuping area, North China Craton: evidence from Petrological and Geochronological data," *Precambrian Research*, vol. 303, pp. 91–104, 2017.

[54] J. H. Qian, C. Q. Yin, J. Zhang, L. Ma, and L. J. Wang, "High-pressure Granulites in the Fuping complex of the central North China Craton: metamorphic P–T–t evolution and Tectonic implications," *Journal of Asian Earth Sciences*, vol. 154, pp. 255–270, 2018.

[55] J. H. Qian, C. Q. Yin, C. J. Wei, and J. Zhang, "Two phases of Paleoproterozoic Metamorphism in the Zhujiafang ductile shear zone of the Hengshan complex: insights into the Tectonic evolution of the North China Craton," *Lithos*, vols. 330–331, pp. 35–54, 2019.

[56] J. H. Qian, C. Q. Yin, S. Li, and J. Zhang, "Metamorphic P–T–t evolution of Amphibolite in the North Hengshan Terrane, North China Craton: insights into the late Paleoproterozoic Tectonic processes from initial collision to final Exhumation," *GSA Bulletin*, vol. 133, nos. 9–10, pp. 2017–2030, 2021.

[57] G.-D. Wang, H. Y. C. Wang, H.-X. Chen, et al., "Metamorphic P–T–t paths of Pelitic Granulites of the Taihua metamorphic complex in the MTS. Huashan area and Tectonothermal implications for the Palaeoproterozoic Trans-North China Orogen," *Precambrian Research*, vol. 290, pp. 147–162, 2017.

[58] J. L. Wu, H. F. Zhang, M. G. Zhai, et al., "Discovery of Pelitic high-pressure Granulite from Manjinggou of the Huai'An complex, North China Craton: metamorphic P–T evolution and geological implications," *Precambrian Research*, vol. 278, pp. 323–336, 2016.

[59] L. L. Xiao, C. M. Wu, G. C. Zhao, J. H. Guo, and L. D. Ren, "Metamorphic P–T paths of the Zanhuang Amphibolites and Metapelites: constraints on the Tectonic evolution of the Paleoproterozoic Trans-North China Orogen," *International Journal of Earth Sciences*, vol. 100, no. 4, pp. 717–739, 2011.

[60] Y. H. Zhang, C. J. Wei, M. J. Lu, and X. W. Zhou, "P–T–t evolution of the high-pressure Mafic Granulites from northern Hengshan, North China Craton: insights from phase Equilibria and Geochronology," *Precambrian Research*, vol. 312, pp. 1–15, 2018.

[61] J. Zhao, L. L. Gou, C. L. Zhang, A. L. Guo, X. J. Guo, and X. Y. Liu, "P–T–t path and Tectonic significance of Pelitic Migmatites from the Lüliang complex in Xiyupi area of Trans-North China Orogen, North China Craton," *Precambrian Research*, vol. 303, pp. 573–589, 2017.

[62] G. C. Zhao, P. A. Cawood, S. Z. Li, et al., "Amalgamation of the North China Craton: key issues and discussion," *Precambrian Research*, vols. 222–223, pp. 55–76, 2012.

[63] L. L. Du, C. H. Yang, L. D. Ren, H. X. Song, Y. S. Geng, and Y. S. Wan, "The 2.2– 2.1 Ga Magmatic event and its Tectonic implication in the Lüliang mountains, North China Craton," *Acta Petrologica Sinica*, vol. 28, no. 9, pp. 2751–2769, 2012.

[64] C. H. Liu, F. L. Liu, and G. C. Zhao, "Provenance and Tectonic setting of the Jiehekou group in the Lüliang complex: constraints from Zircon U–PB age and HF isotopic studies," *Acta Petrologica Sinica*, vol. 29, no. 2, pp. 517–532, 2013.

[65] Y. S. Wan, B. Song, D. Y. Liu, et al., "SHRIMP U–PB Zircon Geochronology of Palaeoproterozoic Metasedimentary rocks in the North China Craton: evidence for a major late Palaeoproterozoic Tectonothermal event," *Precambrian Research*, vol. 149, nos. 3–4, pp. 249–271, 2006.

[66] J. H. Yu, D. Z. Wang, and X. Y. Wang, "Ages of the Lüliang group and its main Metamorphism in the Lüliang mountains, Shanxi: evidence from single grain Zircon U–PB ages," *Chinese Journal of Geochemistry*, vol. 16, no. 2, pp. 170–177, 1997.

[67] J. L. Kang, H. C. Wang, Z. B. Xiao, et al., "Neoarchean Crustal accretion of the North China Craton: evidence from the TTG Gneisses and Monzogranitic Gneisses in Yunzhong mountain area, Shanxi," *Acta Petrologica Sinica*, vol. 33, no. 9, pp. 2881–2898, 2017.

[68] H. C. Wang, J. L. Kang, Z. B. Xiao, et al., "Neoarchean Subduction in North China Craton: new evidence from Themetamorphic high-mg igneous assemblage in Yunzhognshan area, Shanxi province," *Acta Petrologica Sinica*, vol. 34, no. 4, pp. 1099–1118, 2018.

[69] S. W. Liu, Y. M. Pan, J. H. Li, Q. G. Li, and J. Zhang, "Geological and isotopic Geochemical constraints on the evolution of the Fuping complex, North China Craton," *Precambrian Research*, vol. 117, nos. 1–2, pp. 41–56, 2002.

[70] Y. S. Geng, C. H. Yang, and Y. S. Wan, "Paleoproterozoic Granitic Magmatismin the Lüliang area. North China Craton: constraint from isotopic Geochronology," *Acta Petrologica Sinica*, vol. 22, pp. 305–314, 2006.

[71] G. Vavra, D. Gebauer, R. Schmid, and W. Compston, "Multiple Zircon growth and Recrystallization during Polyphase late Carboniferous to Triassic Metamorphism in Granulites of the Ivrea zone (Southern Alps): an ion Microprobe (SHRIMP) study," *Contributions to Mineralogy and Petrology*, vol. 122, no. 4, pp. 337–358, 1996.

[72] A. Polat and A. W. Hofmann, "Alteration and Geochemical patterns in the 3.7–3.8 Ga Isua Greenstone belt, West

Greenland," *Precambrian Research*, vol. 126, nos. 3–4, pp. 197–218, 2003.

[73] B. W. Chappell and A. J. R. White, "Two contrasting granite types," *Pacific Geology*, vol. 8, no. 2, pp. 173–174, 1974.

[74] M. C. Loiselle and D. R. Wones, "Characteristics and origin of Anorogenic Granites," *Geological Society of America, Abstracts with Programs*, vol. 11, p. 468, 1979.

[75] W. J. Collins, S. D. Beams, A. J. R. White, and B. W. Chappell, "Nature and origin of A-type Granites with particular reference to southeastern Australia," *Contributions to Mineralogy and Petrology*, vol. 80, no. 2, pp. 189–200, 1982.

[76] B. Bonin, "Do coeval Mafic and Felsic Magmas in post-Collisional to within-plate regimes necessarily imply two contrasting, Mantle and Crustal, sources? A review," *Lithos*, vol. 78, nos. 1–2, pp. 1–24, 2004.

[77] P. L. King, B. W. Chappell, C. M. Allen, and A. J. R. White, "Are A-type Granites the high temperature Felsic Granites? evidence from fractionated Granites of the Wangrah suite," *Australian Journal of Earth Sciences*, vol. 48, no. 4, pp. 501–514, 2001.

[78] P. L. King, A. J. R. White, B. W. Chappell, and C. M. Allen, "Characterization and origin of Aluminous A-type Granites from the Lachlan fold belt, southeastern Australia," *Journal of Petrology*, vol. 38, no. 3, pp. 371–391, 1997.

[79] J. B. Whalen, K. L. Currie, and B. W. Chappell, "A–type Granites: Geochemical characteristics, discrimination and Petrogenesis," *Contributions to Mineralogy and Petrology*, vol. 95, no. 4, pp. 407–419, 1987.

[80] A. Soesoo, "Fractional crystallization of Mantle-derived melts as a mechanism for some I-type granite Petrogenesis: an example from Lachlan fold belt, Australia," *Journal of the Geological Society*, vol. 157, no. 1, pp. 135–149, 2000.

[81] A. I. S. Kemp, C. J. Hawkesworth, G. L. Foster, et al., "Magmatic and Crustal differentiation history of Granitic rocks from HF–O Isotopes in Zircon," *Science (New York, N.Y.)*, vol. 315, no. 5814, pp. 980–983, 2007.

[82] J. D. Clemens, D. P. F. Darbyshire, and J. Flinders, "Sources of post-Orogenic Calcalkaline Magmas: the Arrochar and Garabal hill–Glen Fyne complexes, Scotland," *Lithos*, vol. 112, nos. 3–4, pp. 524–542, 2009.

[83] M. Bogaerts, B. Scaillet, J.-P. Liégeois, and J. Vander Auwera, "Petrology and geochemistry of the Lyngdal Granodiorite (Southern Norway) and the role of fractional Crystallisation in the genesis of Proterozoic Ferro-Potassic A-type Granites," *Precambrian Research*, vol. 124, nos. 2–4, pp. 149–184, 2003.

[84] C. D. Frost, B. R. Frost, K. R. Chamberlain, and B. R. Edwards, "Petrogenesis of the 1.43 Ga Sherman Batholith, SE Wyoming, USA; a Reducted, Rapakivi-type Anorogenic granite," *Journal of Petrology*, vol. 40, no. 12, pp. 1771–1802, 1999.

[85] J. V. Auwera, M. Bogaerts, J.-P. Liégeois, et al., "Derivation of the 1.0–0.9 Ga A-type Granitoids of Southern Norway by extreme differentiation from Gabbros," *Precambrian Research*, vol. 124, nos. 2–4, pp. 107–148, 2003.

[86] Q. Zhang, W. J. Jin, C. D. Li, Y. Wang, and Y. L. Wang, "Granitic rocks and their formation depth in the crust," *Geotectonica Et Metallogenia*, vol. 35, no. 2, pp. 259–269, 2011.

[87] J. W. Valley, P. D. Kinny, D. J. Schulze, and M. J. Spicuzza, "Zircon Megacrysts from Kimberlite: oxygen Isotope variability among Mantle melts," *Contributions to Mineralogy and Petrology*, vol. 133, nos. 1–2, pp. 1–11, 1998.

[88] A. I. S. Kemp, R. J. Wormald, M. J. Whitehouse, and R. C. Price, "Hf Isotopes in Zircon reveal contrasting sources and crystallization histories for alkaline to Peralkaline Granites of Temora, southeastern Australia," *Geology*, vol. 33, no. 10, 2005.

[89] A. Mushkin, O. Navon, L. Halicz, G. Hartmann, and M. Stein, "The Petrogenesis of A-type Magmas from the Amram Massif, Southern Israel," *Journal of Petrology*, vol. 44, no. 5, pp. 815–832, 2003.

[90] O. Namur, B. Charlier, M. J. Toplis, et al., "Differentiation of Tholeiitic Basalt to A-type granite in the Sept Iles layered intrusion," *Journal of Petrology*, vol. 52, no. 3, pp. 487–539, 2011.

[91] S. P. Turner, J. D. Foden, and R. S. Morrison, "Derivation of some A-type Magmas by fractionation of Basaltic Magma: an example from the Padthaway ridge, South Australia," *Lithos*, vol. 28, no. 2, pp. 151–179, 1992.

[92] B. Landenberger and W. J. Collins, "Derivation of A-type Granites from a dehydrated Charnockitic lower crust: evidence from the Chaelundi complex, Eastern Australia," *Journal of Petrology*, vol. 37, no. 1, pp. 145–170, 1996.

[93] C. D. Frost and B. R. Frost, "On Ferroan (A-type) Granitoids: their compositional variability and modes of origin," *Journal of Petrology*, vol. 52, no. 1, pp. 39–53, 2011.

[94] A. E. Patiño Douce, "Generation of Metaluminous A-type Granites by low-pressure melting of Calc-alkaline Granitoids," *Geology*, vol. 25, no. 8, 1997.

[95] L. M. Cathles, A. H. J. Erendi, and T. Barrie, "How long can a Hydrothermal system be sustained by a single intrusive event?," *Economic Geology*, vol. 92, nos. 7–8, pp. 766–771, 1997.

[96] D. L. Huang, X. L. Wang, X. P. Xia, et al., "Neoproterozoic low-Δ18O Zircons Revisited: implications for Rodinia configuration," *Geophysical Research Letters*, vol. 46, no. 2, pp. 678–688, 2019.

[97] I. N. Bindeman, B. Fu, N. T. Kita, and J. W. Valley, "Origin and evolution of Silicic Magmatism at Yellowstone based on ion Microprobe analysis of Isotopically zone Zircons," *Journal of Petrology*, vol. 49, no. 1, pp. 163–193, 2008.

[98] S. Boroughs, J. A. Wolff, B. S. Ellis, B. Bonnichsen, and P. B. Larson, "Evaluation of models for the origin of Miocene low-Δ18O Rhyolites of the Yellowstone/Columbia river large igneous province," *Earth and Planetary Science Letters*, vols. 313–314, pp. 45–55, 2012.

[99] C. Harris and L. D. Ashwal, "The origin of low-Δ18O Granites and related rocks from the Seychelles," *Contributions to Mineralogy and Petrology*, vol. 143, no. 3, pp. 366–376, 2002.

[100] S. H. Yang, Y. J. Zhao, X. C. Liu, L. Li, and Y. B. Wu, "Tracking partial melting and Protolith nature by Zircon U–PB and HF–O Isotope compositions of Migmatites in the North Dabie Terrane with emphasis on Paleozoic low-Δ18O Magmatism," *GSA Bulletin*, vol. 130, nos. 1–2, pp. 139–153, 2018.

[101] H. P. Taylor, "Oxygen and hydrogen Isotope constraints on the deep circulation of surface waters into zones of Hydrothermal Metamorphism and melting," in *The Role of*

fluids in crustal processes, pp. 72–95, National Academy Press, Washington, DC, 1990.

[102] E. B. Watson and D. J. Cherniak, "Oxygen diffusion in Zircon," *Earth and Planetary Science Letters*, vol. 148, nos. 3–4, pp. 527–544, 1997.

[103] Y. F. Zheng and B. Fu, "Estimation of oxygen Diffusivity from anion porosity in minerals," *GEOCHEMICAL JOURNAL*, vol. 32, no. 2, pp. 71–89, 1998.

[104] I. N. Bindeman and J. W. Valley, "Low-18O Rhyolites from Yellowstone: Magmatic evolution based on analysis of Zircon and individual Phenocrysts," *Journal of Petrology*, vol. 42, no. 8, pp. 1491–1517, 2001.

[105] W. H. Peck, J. W. Valley, and C. M. Graham, "Slow oxygen diffusion rates in igneous Zircons from metamorphic rocks," *American Mineralogist*, vol. 88, no. 7, pp. 1003–1014, 2003.

[106] J. W. Valley, J. R. Chiarenzelli, and J. M. McLelland, "Oxygen Isotope geochemistry of Zircon," *Earth and Planetary Science Letters*, vol. 126, no. 4, pp. 187–206, 1994.

[107] D. Rubatto, "Zircon trace element geochemistry: partitioning with garnet and the link between U–PB ages and Metamorphism," *Chemical Geology*, vol. 184, nos. 1–2, pp. 123–138, 2002.

[108] Taylor, "Water/Rock interactions and the origin of H2O in Granitic Batholiths," *Journal of the Geological Society*, vol. 133, no. 6, pp. 509–558, 1977.

[109] J. Zhao, C. L. Zhang, X. J. Guo, X. Y. Liu, and Q. Wang, "Determination of the 2.4 Ga A-type granite in Lüliang area of the North China Craton and its geological significance," *Acta Petrologica Sinica*, vol. 31, no. 6, pp. 1606–1620, 2015.

[110] C. H. Liu, G. C. Zhao, F. L. Liu, and W. Xu, "Coexistence of A- and I-type Granites in the Luliang complex: Tectonic implications for the middle Paleoproterozoic Trans-North China Orogen, North China Craton," *Lithos*, vols. 380–381, p. 105875, 2021.

[111] Q. Y. Yang and M. Santosh, "Charnockite Magmatism during a transitional phase: implications for late Paleoproterozoic ridge Subduction in the North China Craton," *Precambrian Research*, vol. 261, pp. 188–216, 2015.

[112] J. Zhao, C. L. Zhang, X. Y. Liu, and J. Gan, "Middle Paleoproterozoic Tectonic evolution of the Trans-North China Orogen, North China Craton: constraint from the intermediate–acid Magmatism in the Lüliang area," *Lithosphere*, vol. 105804, pp. 378–379, 2020.

[113] J. Zhao, C. L. Zhang, X. J. Guo, and X. Y. Liu, "The late-Paleoproterozoic I- and A-type Granites in Lüliang complex, North China Craton: new evidence on post-Collisional extension of Trans-North China Orogen," *Precambrian Research*, vol. 318, pp. 70–88, 2018.

[114] A. B. Thompson, "Sometime-space relationships for Crustal melting and Granitic intrusion at various depths," *Geological Society, London, Special Publications*, vol. 168, no. 1, pp. 7–25, 1999.

[115] W. J. Collins, "Hot Orogens, Tectonic switching, and creation of Continental crust," *Geology*, vol. 30, no. 6, 2002.

[116] Z. Garfunkel, C. A. Anderson, and G. Schubert, "Mantle circulation and the lateral migration of Subducted slabs," *Journal of Geophysical Research*, vol. 91, no. B7, pp. 7205–7223, 1986.

[117] G. N. Eby, "Chemical subdivision of the A-type Granitoids: Petrogenetic and Tectonic implications," *Geology*, vol. 20, no. 7, 1992.

[118] L. L. Du, C. H. Yang, W. Wang, et al., "Paleoproterozoic Rifting of the North China Craton: Geochemical and Zircon HF isotopic evidence from the 2137 ma Huangjinshan A-type granite Porphyry in the Wutai area, " *Journal of Asian Earth Sciences*, vol. 72, pp. 190–202, 2013.

[119] J. L. Wang, C. H. Yang, D. A. Wyman, H. X. Song, and L. L. Du, "Petrogenesis and Tectonic implications of the 2.1–2.0 Ga Granitoids in Fuping complex, North China Craton: constraints from Petrology, geochemistry and Zircon U–PB–HF Isotopes," *Precambrian Research*, vol. 339, 2020.

[120] L. Du, C. Yang, D. A. Wyman, et al., "2090–2070 ma A-type Granitoids in Zanhuang complex: further evidence on a Paleoproterozoic rift-related Tectonic regime in the Trans-North China Orogen," *Lithos*, vols. 254–255, pp. 18–35, 2016.

[121] Y. S. Wan, D. Y. Liu, S. J. Wang, et al., "~2.7 Ga juvenile crust formation in the North China Craton (Taishan–Xintaiarea, Western Shandong province): further evidence of an understated event from U–PB dating and HF isotopic composition of Zircon," *Precambrian Research*, vol. 186, nos. 1–4, pp. 169–180, 2011.

[122] Y. S. Wan, C. Y. Dong, P. Ren, et al., "Spatial and temporal distribution, compositional characteristics and formation and evolution of Archean TTG rocks in the North China Craton: Asynthesis," *Acta Petrologica Sinica*, vol. 33, no. 5, pp. 1405–1419, 2017.

[123] S. A. Wilde and G. Zhao, "Late Archean to Paleoproterozoic evolution of the North China Craton: key issues Revisited," *Journal of Asian Earth Sciences*, vol. 24, no. 5, pp. 519–522, 2005.

[124] P. D. Maniar and P. M. Piccoli, "Tectonic discrimination of Granitoids," *Geological Society of America Bulletin*, vol. 101, no. 5, pp. 635–643, 1989.

[125] A. Streckeisen, "Classification and nomenclature of plutonic rocks recommendations of the IUGS Subcommission on the SYSTEMATICS of igneous rocks," *Geologische Rundschau*, vol. 63, no. 2, pp. 773–786, 1974.

[126] B. M. Wilson, "Igneous Petrogenesis," in *Igneous Petrogenesis a Global Tectonic Approach*, Springer, Dordrecht, 1989. http://link.springer.com/10.1007/978-1-4020-6788-4.

[127] S. -s. Sun and W. F. McDonough, "Chemical and isotopic SYSTEMATICS of Oceanic Basalts: implications for Mantle composition and processes," *Geological Society, London, Special Publications*, vol. 42, no. 1, pp. 313–345, 1989.

[128] R. Y. Zhang, C. L. Zhang, C. R. Diwu, and Y. Sun, "Zircon U–PB Geochronology, geochemistry and its geological implications for the Precambrian Granitoids in Zhongtiao mountain, Shanxi province," *Acta Petrologica Sinica*, vol. 28, no. 11, pp. 3559–3573, 2012.

[129] B. Chen, S. W. Liu, Y. S. Geng, and C. Q. Liu, "Hf Isotopes and significance of the late Archean–Paleoproterozoic Granitoids from the Wutai–Lüliang terrain, North China," *Acta Petrologica Sinica*, vol. 22, no. 2, pp. 296–304, 2006.

[130] L. L. Du, C. H. Yang, H. X. Song, et al., "Petrogenesis and Tectonic setting of 2.2–2.1 Ga Granites in Wutai area, North China Craton," *Acta Petrologica Sinica*, vol. 34, no. 4, pp. 1154–1174, 2018.

[131] G. H. Hu, Y. Y. Zhou, S. H. Zhang, W. Wang, T. P. Zhao, and S. Y. Wang, "Petrogenesis and metamorphic age of Palaeoproterozoic Granitic Gneisses in Lüliang area: constraints from Zircon and Monazite U–PB ages and HF Isotopes," *Acta Petrologica Sinica*, vol. 36, no. 12, pp. 3631–3653, 2020.

[132] Q. Li, M. Santosh, S. R. Li, and P. Guo, "The formation and rejuvenation of Continental crust in the central North China Craton: evidence from Zircon U–PB Geochronology and HF Isotope," *Journal of Asian Earth Sciences*, vol. 95, no. 1, pp. 17–32, 2014.

[133] L. Tang, M. Santosh, and X. M. Teng, "Paleoproterozoic (ca. 2.1–2.0 Ga) arc Magmatism in the Fuping complex: implications for the Tectonic evolution of the Trans-North China Orogen," *Precambrian Research*, vol. 268, pp. 16–32, 2015.

[134] C. Wang, S. G. Song, M. B. Allen, L. Su, G. C. Zhao, and T. Y. Gao, "Late Paleoproterozoic Magmatism in North Hengshan: final collapse of the Trans-North China Orogen," *Precambrian Research*, vol. 374, 2022.

[135] X. Q. Yu, J. L. Liu, C. L. Li, S. Q. Chen, and Y. P. Dai, "Zircon U–PB dating and HF Isotope analysis on the Taihua complex: constraints on the formation and evolution of the Trans-North China Orogen," *Precambrian Research*, vol. 230, pp. 31–44, 2013.

[136] R. Y. Zhang, C. L. Zhang, and Y. Sun, "Crustal Reworking in the North China Craton at similar to 2.5 Ga: evidence from Zircon U–PB ages, HF Isotopes and whole–rock geochemistry of the TTG Gneisses in the Zhongtiao mountain," *Acta Petrologica Sinica*, vol. 29, no. 7, pp. 2265–2280, 2013.

[137] R. F. Zhao, J. H. Guo, P. Peng, and F. Liu, "2.1 Ga Crustal Remelting event in Hengshan complex: evidence from Zircon U–PB dating and HF–nd isotopic study on Potassic Granites," *Acta Petrologica Sinica*, vol. 27, no. 6, pp. 1607–1623, 2011.

[138] J. Blichert-Toft and F. Albarède, "The LU–HF geochemistry of Chondrites and the evolution of the Mantle–crust system," *Earth and Planetary Science Letters*, vol. 148, nos. 1–2, pp. 243–258, 1997.

[139] C. H. Yang, L. L. Du, L. D. Ren, H. X. Song, H. Q. Xie, and Z. X. Liu, "The age and Petrogenesis of the Xuting granite in the Zanhuang complex, Hebei province: constraints on the structural evolution of the Trans–North China Orogen, North China Craton," *Acta Petrologica Sinica*, vol. 27, no. 4, pp. 1003–1016, 2011.

[140] X. Q. Deng, T. P. Peng, T. P. Zhao, and Z. L. Qiu, "Petrogenesis of the late Paleoproterozoic (similar to 1.84 Ga) Yuantou A-type granite in the Southern margin of the North China Craton and its Tectonic implications," *Acta Petrologica Sinica*, vol. 35, no. 8, pp. 2455–2469, 2019.

[141] M. S. Mu, D. B. Yang, H. T. Yang, et al., "Petrogenesis of late Paleoproterozoic post-Collisional Magmatism in Southern North China Craton: insights from geochemistry and nd–HF isotopic compositions of A-type Granites," *Precambrian Research*, vol. 383, 2022.

[142] S. Xue, Y. Xu, M. X. Ling, et al., "Geochemical constraints on genesis of Paleoproterozoic A-type granite in the South margin of North China Craton," *Lithos*, vols. 304–307, pp. 489–500, 2018.

[143] X. Q. Deng, T. P. Peng, and T. P. Zhao, "Geochronology and geochemistry of the late Paleoproterozoic Aluminous A-type granite in the Xiaoqinling area along the Southern margin of the North China Craton: Petrogenesis and Tectonic implications," *Precambrian Research*, vol. 285, pp. 127–146, 2016.

[144] J. P. Shi, D. B. Yang, T. F. Huo, H. T. Yang, W. L. Xu, and F. Wang, "The Geochronology and nd–HF Isotope compositions of A-type Granites on the Southern margin of North China Craton: constraints on the late Paleoproterozoic Extensional events," *Acta Petrologica Sinica*, vol. 33, no. 10, pp. 3042–3056, 2017.